REFERENCES

Benjamin, S. G., G. A. Grell, J. M. Brown, T. G. Smirnova, and R. Bleck, 2004a: Mesoscale weather prediction with the RUC hybrid isentropic-terrain-following coordinate model. *Mon. Wea. Rev.*, *132,* 473–494.

Benjamin, S. G., D. Dévényi, S. S. Weygandt, K. J. Brundage, J. M. Brown, G. A. Grell, D. Kim, B. E. Schwartz, T. G. Smirnova, T. L. Smith, and G. S. Manikin, 2004b: An hourly assimilation-forecast cycle: The RUC. *Mon. Wea. Rev.*, *132,* 495–518.

Brooks, D. R., and F. M. Mims III, 2001: Development of an inexpensive handheld LED-based Sun photometer for the GLOBE program. *J. Geophys. Res., 106(D5),* 4733–4740.

COMET, 2002: Satellite meteorology: GOES channel selection. http://meted.ucar.edu/satmet/goeschan/print/print.htm

Duda, D. P., P. Minnis, L. Nguyen, R. Palikonda, 2004: A case study of the development of contrail clusters over the Great Lakes. *J. Atmos. Sci.*, *61,* 1132–1146.

Glahn, H. R., D. A. Lowry, 1972: The use of model output statistics (MOS) in objective weather forecasting. *J. Appl. Meteorol., 11,* 1203–1211.

Hosmer, D. W., and S. Lemeshow, 1989: *Applied Logistic Regression.* John Wiley & Sons, New York, 307 pp.

Jackson, A., B. Newton, D. Hahn, A. Bussey, 2001: Statistical contrail forecasting. *J. Appl. Meteorol., 40,* 269–279.

Jensen, E. J., A. S. Ackerman, D. E. Stevens, O. B. Toon, and P. Minnis, 1998: Spreading and growth of contrails in a sheared environment. *J. Geophys. Res., 103,* 31,557–31,567.

Keith, R., 2003: Optimization of value of aerodrome forecasts. *Weather and Forecasting, 18,* 808–824.

Lund, I. A., 1955: Estimating the probability of a future event form dichotomously classified predictors. *Bull. Amer. Meteorol. Soc., 36,* 325–328.

Mannstein, H., R. Meyer, P. Wendling, 1999: Operational detection of contrails from NOAA-AVHRR data. *Int. J. Remote Sensing, 20,* 1641–1660.

Schumann, U., 1996: On conditions for contrail formation from aircraft exhausts. *Meteorologische Zeitschrift, 5,* 4–23.

Travis, D. J., A. M. Carleton, S. A. Changnon, 1997: An empirical model to predict widespread occurrences of contrails. *J. Appl. Meteor., 36,* 1211–1220.

Walters, M. K., J. D. Shull, J. P. Asbury III, 2000: A comparison of exhaust condensation trail forecast algorithms at low relative humidity. *J. Appl. Meteor., 39,* 80–91.

Wilks, D. S., 1995: *Statistical Methods in the Atmospheric Sciences.* Academic Press, 467 pp.

Xue, M., D. –H. Wang, J. –D. Gao, K. Brewster, and K. K. Droegemeier, 2003: The Advanced Regional Prediction System (ARPS), storm-scale numerical weather prediction and data assimilation. *Meteor. Atmos. Physics, 82,* 139–170.

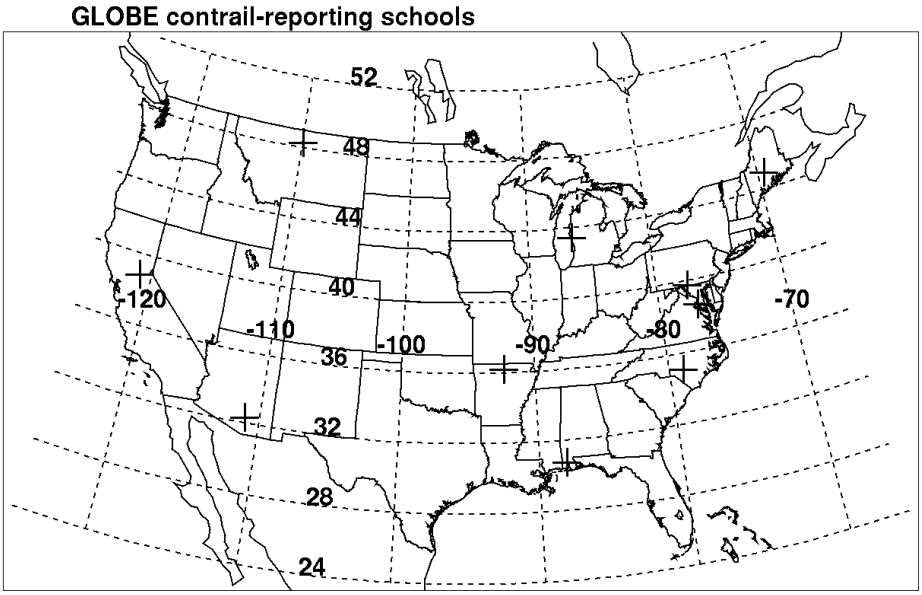

Figure 1: Location of contrail-reporting schools in the United States of America used in the development of logistic regression models.

Climate sensitivity of radiative impacts from transport systems

M. Ponater*, V. Grewe, R. Sausen, U. Schumann
DLR-Institut für Physik der Atmosphäre, Oberpfaffenhofen, Germany

S. Pechtl
Institut für Umweltphysik der Universität Heidelberg, Germany

E. J. Highwood, N. Stuber
Department of Meteorology, University of Reading, UK

Keywords: Efficacy, Climate Sensitivity, Aviation Climate Impact

ABSTRACT: Comparing individual components of a total climate impact is traditionally done in terms of radiative forcing. However, the climate impact of transport systems includes contributions that are likely to imply climate sensitivity parameters distinctly different from the "reference value" for a homogeneous CO_2 perturbation. We propose to introduce efficacy factors for each component into the assessment. The way of proceeding is illustrated using aviation as an example, and prospects for evaluating the other transport system in the EU project QUANTIFY are given.

1 INTRODUCTION

The traditional way to compare the global climate impact of individual emission sectors, as well as specific contributions forming the total effect of some emission sector, is the radiative forcing (RF, Shine et al., 1990). RF is easily calculated by means of radiative transfer models and provides meaningful results even for very small perturbations that are unable to force statistically significant response signals in three-dimensional climate models. RF is also less model-dependent than other metrics of climate change (like the response of surface temperature, precipitation, storminess etc.), because the complex (in part poorly understood) feedbacks within the climate system (cp., Bony et al., 2006) do not enter the radiative transfer calculations. Such practical advantages make RF (and its derivatives like, e.g., the global warming potential, GWP) a seemingly ideal metric for assessment purposes. Consequently, RF and GWP have formed the basis of established emission trading systems.

As research on the climate impact of distinctly non-homogeneous forcing agents (like aerosols, ozone, or clouds induced by aircraft or ships) has received mounting interest, doubts have increased concerning the adequacy of RF for intercomparing relative impacts (e.g., Hansen et al., 1997, 2005; Cook and Highwood, 2003; Joshi et al., 2003; Stuber et al., 2005; Ponater et al., 2005). Here, we will discuss the concept of the EU project QUANTIFY to assess the climate impact contributions from transport systems in the light of current caveats in using RF as a respective metric.

2 CLIMATE SENSITIVITY

The idea to use RF as a metric for the climate change to be expected from some forcing origins from a recurrent empirical finding in climate modelling. Such experience has suggested a linear relation,

$$\Delta T_{surf} = \lambda \cdot RF \,, \qquad (1)$$

* *Corresponding author:* Michael Ponater, DLR-Institut für Physik der Atmosphäre, Oberpfaffenhofen, D-82230 Wessling, Germany. Email: michael.ponater@dlr.de

between the global mean surface temperature response, ΔT_{surf}, and global mean radiative forcing, *RF*. The relating climate sensitivity parameter, λ, can be, with reasonable reliability, assumed to be independent of the nature of the forcing agent, i.e., its magnitude, longwave to shortwave spectral distribution, spatial structure, or seasonal variation. While λ is known to vary between different climate models, mainly due to a considerable model dependency of cloud feedbacks (Cess et al., 1989, 1996), many simulations implying changes of CO_2 concentration, other well-mixed greenhouse gases, or of the solar constant have confirmed the basic assumption within one and the same model configuration. Consequently, once the value of λ has been determined for the CO_2 case, it is then considered as a model constant applicable to all other agents. However, evidence is growing (see papers mentioned in the introduction) that this approach may fail on several occasions.

Table 1: Equilibrium climate sensitivity parameters (λ) as determined from ECHAM4 simulations. Global changes of CH_4, solar constant, CO_2, and ozone in the middle troposphere (MT), upper troposphere (UT), and lower stratosphere (LS) have been used as horizontally homogeneous forcing perturbations. The latter four agents have also been applied as a forcing restricted to the northern hemisphere extratropics (last two columns). See Stuber et al. (2005), for more details.

Agent	RF (Wm^{-2})	λ (K/Wm^{-2})	RF (Wm^{-2})	λ (K/Wm^{-2})
	Global perturbation		NH extratropics perturbation	
CO_2	1.0	0.81	1.0	1.12
Solar	1.0	0.82		
CH_4	1.0	0.88		
O_3(MT)	1.0	0.92	1.0	1.10
O_3(UT)	1.0	0.58	1.0	0.87
O_3(LS)	1.0	1.46	1.0	1.83

Table 1 gives an overview over equilibrium climate change simulations that have been conducted with the ECHAM4/T30.L19 climate model coupled to a mixed layer ocean module. The climate sensitivity parameter has been determined for a number of radiative perturbations, all normalised to a global mean of RF=1 W/m^2. While the conventional perturbations behave more or less in line with the assumption of constant climate sensitivity, there is a clear tendency to higher sensitivity for perturbation impacting on the northern hemisphere extratropics (Joshi et al., 2003). Compared to the reference value for CO_2, ozone has a distinctly higher sensitivity if the change occurs in the lower stratosphere, whereas the sensitivity is smaller for changes in the upper troposphere (Stuber et al., 2005). It is evident that non-homogeneous forcings may trigger specific feedbacks that are either less distinguished or less variable in the case of homogeneous forcings.

If the experience from non-homogeneous ozone perturbations already poses a challenge for the concept of constant climate sensitivity, simulations for non-homogeneous aerosol perturbations produce most embarrassing results: Table 2 recalls climate sensitivity experiments conducted by Cook and Highwood (2003) with the UREAD climate model of intermediate complexity. Forcing agents were scattering and absorbing aerosols in the lower troposphere (LT), the varied parameter was the aerosol single scattering albedo, ω.

Table 2: Climate sensitivity results from the UREAD climate model. Global horizontally homogeneous aerosol distribution, with fixed optical depth and asymmetry factor but varying single scattering albedo (ω) have been used as the forcing agent (see Cook and Highwood, 2003, for details).

Agent	ΔT_{surf} (K)	RF (Wm^{-2})	λ (K/Wm^{-2})
CO_2	1.9	3.81	0.50
Aero (LT), ω=1	-1.70	-4.72	0.36
Aero (LT), ω=0.95	-0.60	-3.02	0.20
Aero (LT), ω=0.9	0.60	-1.40	-0.43
Aero (LT), ω=0.85	1.80	0.14	12.86
Aero (LT), ω=0.8	2.90	1.61	1.80

Scattering aerosols (ω=1) cause negative RF and a surface cooling, yielding a climate sensitivity parameter smaller but still in the vicinity of the reference value for CO_2. As the absorbing character of the aerosol increases the λ values get more anomalous, culminating at negative λ for a critical single scattering albedo around ω=0.9, for which negative RF even causes a rise of global surface

temperature. As pointed out by Cook and Highwood (2003) the reason for the irregular sensitivity in this case is the feedback on lower troposphere cloud cover (the "semi-direct aerosol effect"), which markedly decreases as a result of absorption heating. Due to some observational evidence indicating distinguished impacts of lower tropospheric aerosols on the hydrological cycle (e.g., Ramanathan et al., 2005), the semi-direct effect is not likely to be a mere model feature.

Summarising, climate model simulations with idealised non-homogeneous forcing agents suggest deviations from the reference climate sensitivity that are too strong to be ignored if, for example, ozone, aerosol, and CO_2 contributions to a total effect are to be compared. A way to account this for is the inclusion of efficacy factors (Hansen et al., 2005) in equation (1), writing instead

$$\Delta T^{(i)}{}_{surf} = r_i \cdot \lambda_{CO2} \cdot RF^{(i)} \qquad (2)$$

where $r_i=\lambda_i/\lambda_{CO2}$ would introduce the knowledge on an anomalous climate sensitivity λ_i for the component contributing the forcing $RF^{(i)}$. Quantifying individual components in terms of $\Delta T^{(i)}{}_{surf}$ rather than $RF^{(i)}$ may be expected to provide a fairer, more reliable, assessment. Introducing efficacy factors in this way is encouraged by the finding that the model dependence of those factors seems to be smaller than the model dependence of the climate sensitivity parameter itself (Hansen et al., 1997; Joshi et al., 2003). Another favourable point to mention is the possibility to include efficacies into the calculation of GWPs (Fuglestvedt et al., 2003; Berntsen et al., 2005) or into other linear extensions of the radiative forcing concept (e.g., Ponater et al., 2006).

3 EFFICACY OF AIRCRAFT CLIMATE IMPACT COMPONENTS – A TEST CASE

Compared to other transport sectors knowledge on the climate impact from aircraft is relatively far advanced. RF values for the various contributions were first quantified for an IPCC special report (Penner et al. 1999) and improved by subsequent research work. However, aviation effects beyond CO_2 and CH_4 just exhibit the properties that make anomalous climate sensitivity likely to occur: They are non-homogeneous in time and space (both horizontally and vertically). We have performed a series of equilibrium climate change simulations with the ECHAM4/T30.L39(DLR) climate model, in order to determine climate sensitivity parameters separately for each impact component (Ponater et al., 2005; 2006). It is important to note that the calculation of a statistically significant surface temperature response (ΔT_{surf}) requires, in most cases, a scaling of the forcing perturbation, as the unscaled RFs generally range well below 0.1 Wm^{-2} for present day conditions (Penner et al., 1999; Sausen et al., 2005). The results for the individual climate sensitivity and efficacy values are shown in Table 3:

Table 3: Results (global annual averages) from aircraft climate sensitivity simulations. CO_2 and CH_4 perturbations were normalised to 1 Wm^{-2}. Two aircraft O_3 perturbations of the Grewe et al. (2002, their Fig. 3) type (i.e., for year 2015) were used in two separate simulations. The perturbations for contrails and for H_2O were artificially scaled by factors between 50 and 80, relative to actua1 present day conditions. See Ponater et al. (2005, 2006) for more details.

	CO_2	CH_4	$O_3(1)$	$O_3(2)$	H_2O	contrails
RF (Wm^{-2})	1.00	1.00	0.059	0.062	0.06	0.19
ΔT_{surf} (K)	0.74	0.86	0.060	0.071	0.05	0.08
λ (K/ Wm^{-2})	0.74	0.86	1.02	1.15	0.83	0.43
r	1	1.18	1.37	1.55	1.14	0.59

As expected some *r* values differ significantly from unity. Aircraft ozone changes have a by 40 % higher efficacy, while the climate sensitivity of contrails is considerably lower than the reference value. Figure 1 shows the corresponding zonal mean RFs, and zonal mean cross sections of the atmospheric temperature response. Note the specific characteristics of aircraft ozone, water vapour, and contrail perturbations with respect to the latitudinal profile and the combination of longwave and shortwave radiative components. Moreover, contrail RF is extremely variable on short time scales, and ozone RF includes strong seasonal variability. While we emphasise that equations (1) and (2) may be applied only for global and annual means, the three-dimensional climate simulations basic to the averaged values of Table 3 offer ample opportunity to investigate local forcings and feedbacks and to discuss their relevance for the global response in each case (e.g., Stuber et al.,

2005; Ponater et al., 2005). Still, the current level of process understanding needs to be advanced and available knowledge on, e.g., model dependency issues is very sparse. In particular, important aspects of the interaction between aerosols, clouds and radiation are little explored. Even the sign of the indirect impact of aircraft emitted soot on climate is currently unknown (Hendricks et al., 2005).

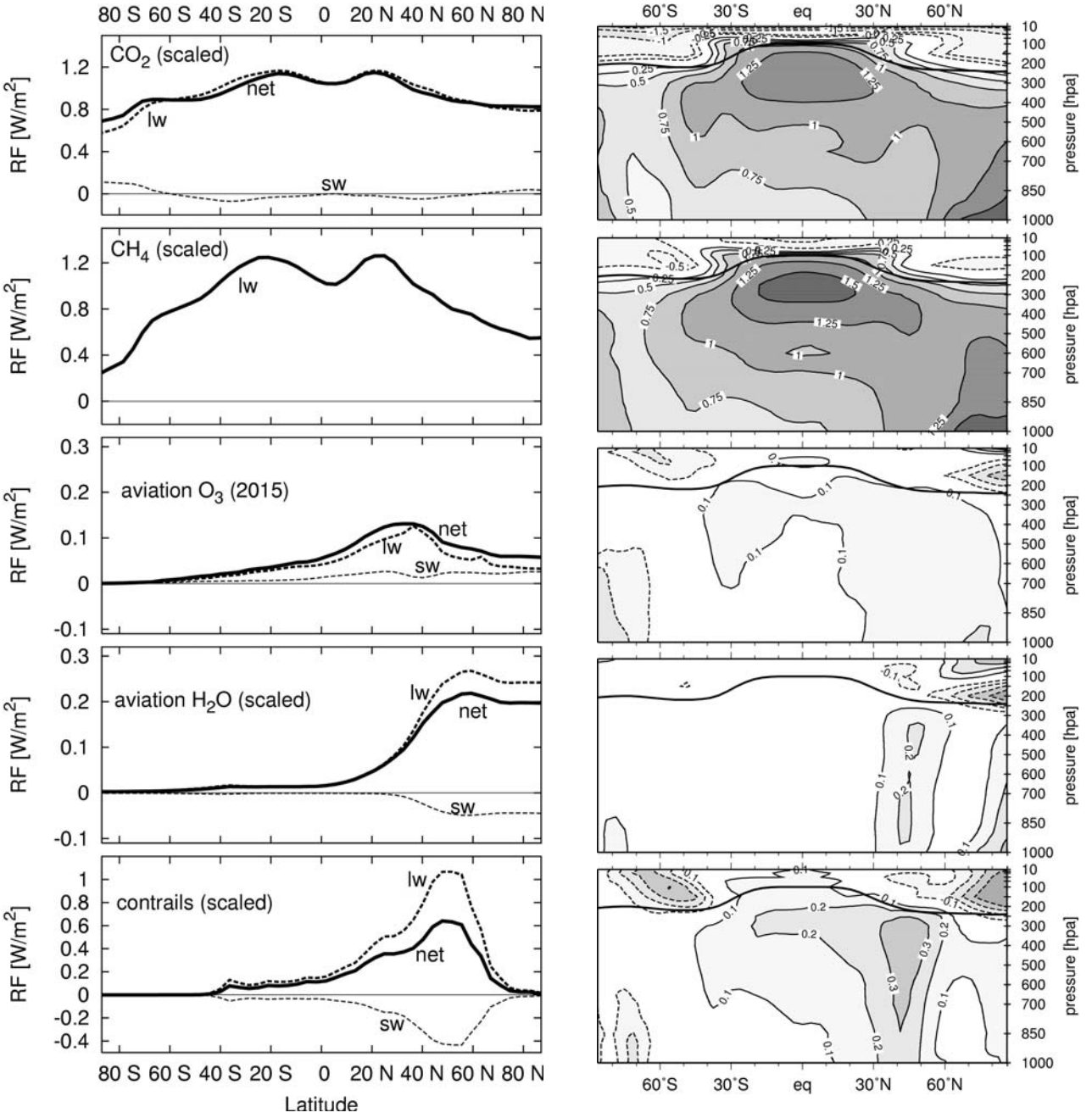

Figure 1: Zonal mean radiative forcing profile (Wm^{-2}, left) and zonal mean temperature reponse (in K, right) caused by various aircraft impact components as simulated with the ECHAM4 GCM. Note that the actual aircraft induced perturbations had to be scaled (see Table 3, and main text). Annual averages of forcing and response are shown. The essential part of the temperature response is statistically significant.

4 EFFICACY OF TRANSPORT CLIMATE COMPONENTS

The generalisation of the efficacy concept outlined in Section 2 to all transport related emissions, as it is intended in the QUANTIFY project, will add further complexity. First, aerosol induced forcings and feedbacks form a main part of the total effect for surface sources (this is particularly true for ships), and it is largely unknown how the aerosol-cloud interaction effects discussed in the context of Table 2 will manifest globally, if the perturbations are restricted to certain geographical re-

gions. This subject will be one of the central issues in QUANTIFY. Second, for both aerosols and ozone the individual spatial structure of the perturbation is likely to create an individual efficacy value. Figure 2 illustrates how different, e.g., the ozone change patterns of the different sectors of transport can be expected to be, and in view of the results shown in Table 1 this is almost certain to modify the climate sensitivity. However, if the approach we follow is to make sense, the climate sensitivity must remain well-defined, in reasonable limits, for each contributing perturbation.

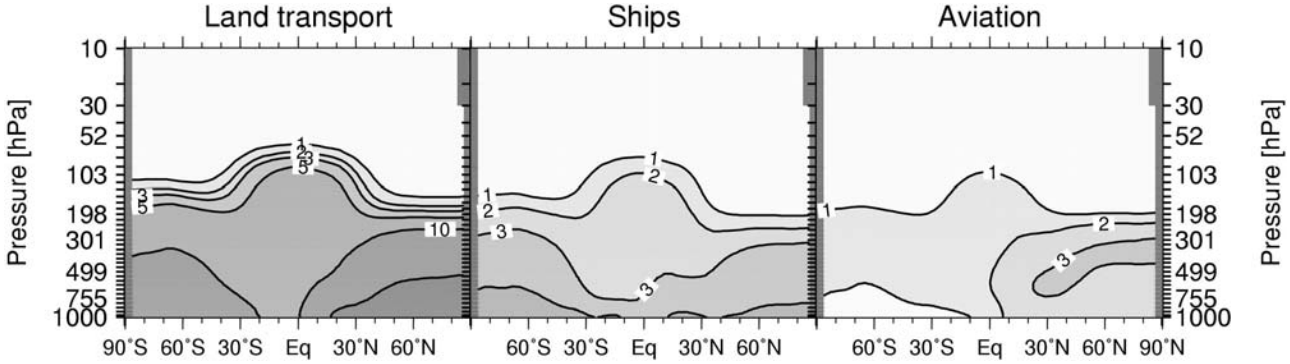

Figure 2: Annual mean ozone change induced by NO_x emissions from road transport, ship transport, and aviation, for typical 1990ies conditions. Values indicate fraction of the total ozone concentration (in %). Results are extracted from the interactive chemistry-climate model simulation discussed by Dameris et al. (2005) Contributions from individual NO_x sources were separated according to the Grewe (2004) method. Contour lines are 1, 2, 3, 5, 10, 20 %.

This requires, above all, a high degree of linearity for each contribution, i.e., the efficacy values in equation (2) must not depend significantly on the magnitude of RF. Otherwise any scaling, as has been done for the aviation perturbations discussed in Section 3, is prohibited and our concept would be bound to fail. Therefore, extra linearity checks are intended in QUANTIFY. Third, if distinctive efficacy values can indeed be determined for each contribution it will be necessary to identify the degree of additivity, if the components are recombined to yield an efficacy for the total effect (either for each single transport sector, or for the gross effect of total transport). Respective non-linearities have been reported, e.g. for the overall interaction of greenhouse gas and aerosol forcing (Feichter et al., 2004). If such evidence consolidates, a sufficient understanding must be developed in order to arrive at a reasonable synthesis of the separate forcing, efficacy, and response results, and in order to eventually convert our knowledge of climate interaction processes to assessment numbers that are reliable enough to be translated into damage functions or other measures of socio-economic impact (see contribution by Shine, this volume).

REFERENCES

Berntsen, T.K. et al., 2005: Response of climate to regional emissions of ozone precursors: sensitivities and warming potentials. Tellus 57B, 283-304.

Bony, S., R. Colman, V.M. Kattsov, et al., 2006: How Well Do We Understand and Evaluate Climate Change Feedback Processes? J. Clim. 19, 3445-3481.

Cess, R.D., G.L. Potter, et al., 1989: Interpretation of Cloud-Climate Feedback as Produced by 14 Atmospheric General Circulation Models, Science 245, 513-516.

Cess, R.D., M.-H. Zhang, W.J. Ingram, G.L. Potter, et al., 1996: Cloud feedback in atmospheric general circulation models: An update. J. Geophys. Res. 101, 12791-12794.

Cook, J. and E.J. Highwood, 2003: Climate response to tropospheric absorbing aerosols in an intermediate general-circulation model. Q. J. R. Meteorol. Soc. 130, 175-191.

Dameris, M., et al., 2005: Long-term changes and variability in a transient simulation with a chemistry-climate model employing realistic forcing. Atmos. Chem. Phys. 5, 2121-2145.

Feichter, J., E. Roeckner, U. Lohmann, and B. Liepert, 2004: Nonlinear Aspects of the Climate Response to Greenhouse Gas and Aerosol Forcing. J. Clim. 17, 2384-2398.

Fuglestvedt, J.S., T.K., Berntsen, O. Godal, R. Sausen, K.P. Shine, and T. Skodvin, 2003: Metrics of climate change: Assessing radiative forcing and emission indices. Clim. Change 58, 267-331.

Grewe, V., M. Dameris, C. Fichter, and R. Sausen, 2002: Impact of aircraft NO_x emissions. Part 1: Interactively coupled climate-chemistry simulations and sensitivities to climate feedback, lightning, and model resolution. Meteorol. Z. 11, 177-186.

Grewe, V., 2004: Technical Note: A diagnostic for ozone contributions of various NO_x emissions in multi-decadal chemistry-climate model simulations. Atmos. Chem. Phys. 4, 729-736.

Hansen, J., M. Sato, and R. Ruedy, 1997: Radiative forcing and climate response. J. Geophys. Res. 102, 6831-6864.

Hansen, J., M. Sato, R. Ruedy, L. Nazarenko, A. Lacis, G.A. Schmidt, G. Russell, et al., 2005: Efficacy of climate forcings. J. Geophys. Res. 110, D18104, doi:10.1029/2005GL022740.

Hendricks, J., B. Kärcher, U. Lohmann, and M. Ponater, 2005: Do aircraft black carbon emissions affect cirrus clouds on the global scale? Geophys. Res. Lett. 32, L12814, doi:10.1029/2005GL022740.

Joshi, M.M., K.P. Shine, M. Ponater, N. Stuber, R. Sausen, and L. Li, 2003: A comparison of climate response to different radiative forcings in three general circulation models: towards an improved metric of climate change. Clim. Dyn. 20, 843-854, doi:10.1007/s00382-003-0305-9.

Penner, J.E., D.H. Lister, D.J. Griggs, D.J. Dokken, M. McFarland (eds.), 1999: Intergovernmental Panel on Climate Change (IPCC) special report *Aviation and the Global Atmosphere*. Cambridge University Press, New York, 365pp.

Ponater, M., S. Marquart, R. Sausen, and U. Schumann, 2005: On contrail climate sensitivity. Geophys. Res. Lett. 32, L10706, doi:10.1029/2005GL022580.

Ponater, M., S. Pechtl, R. Sausen, U. Schumann, and G. Hüttig, 2006: Potential of the cryoplane technology to reduce aircraft climate impact: A state-of-the-art assessment. Atmos. Environ. 40, 6928-6944, doi:10.1016/ j.atmosenv.2006.06.036.

Ramanathan, V., C. Chung, D. Kim, T. Bettge, L. Buja, J.T. Kiehl, W.M. Washington, Q. Fu, and D.R. Sikka, 2005: Atmospheric brown clouds: Impacts on South Asian climate and hydrological cycle. Proc. Nat. Acad. Sci. 102, 5326-5333, doi:10.1073/pnas.0500656102.

Sausen, R., I. Isaksen, V. Grewe, D. Hauglustaine, D.S. Lee, G. Myhre, M.O. Köhler, G. Pitari, U. Schumann, F. Stordal, and C. Zerefos, 2005: Aviation radiative forcing in 2000: An update on IPCC (1999). Meteorol. Z. 14, 555-561, doi:10.1127/0941-2948/2005/0049.

Shine, K.P., R.G. Derwent, D.J. Wuebbles, and J.-J. Morcrette, 1990: Radiative Forcing of Climate. In: Houghton, J.T. et al. (eds.), Climate Change: The IPCC Scientific Assessment. Cambridge University Press, New York, 41-68.

Stuber, N., M. Ponater, and R. Sausen, 2005: Why radiative forcing might fail as a predictor of climate change. Clim. Dyn. 24, 497-510, doi:10-1007/s00382-004-0497-7.

Results from pulse scenario experiments with the CNRM-CM3 global coupled model

D. Olivié*, H. Teyssèdre, D. Salas-Mélia, J.-F. Royer, F. Karcher
Centre National de Recherches Météorologiques (CNRM), Toulouse, France

D. Cariolle
Centre Européen de Recherches et de Formation Avancée en Calcul Scientifique (CERFACS),Toulouse, France

Keywords: simple climate model, coupled climate model, climate change, CO_2, solar constant, response time

ABSTRACT: In order to validate Simple Climate Models (SCMs), the response of the Atmosphere Ocean General Circulation Model (AOGCM) CNRM-CM3 to specific forcing scenarios is studied. Upon pre-industrial background conditions, a sudden perturbation in the solar constant or the CO_2 concentration was applied, followed by an exponential decay of the perturbation. Identical experiments performed with SCMs allow than a validation of the SCMs parameters.

The CNRM-CM3 model is a global coupled climate model which consists of an atmosphere general circulation model, an ocean general circulation model, and a sea ice model. In addition to the validation of SCMs, these experiments can also be used to better understand the characteristics of AOGCMs. The atmosphere and ocean show clearly distinct response times to the forcings. Where the response time for the atmosphere is between 5 and 10 year, the response time for the ocean varies between 60 and 120 year. Furthermore, the influence of the initial conditions is not very large and the response time of the ocean is not very robust with respect to the length of the perturbation.

Comparison with results from earlier simulations with the CNRM-CM3 model where the CO_2 concentration was increased in a gradual way show that, although the forcing scenarios used in these new simulations are strongly transient, they can give valuable information about the characteristics of the model.

1 INTRODUCTION

AOGCMs are the most accurate models to study the effect of different emission scenarios on the Earths climate. However, these models are too computationally expensive to be used for large sets of emission scenarios. Simple Climate Models (SCMs) which are computationally less expensive (and therefore also less accurate) can be used to study the impact of a large set of emission scenarios. Such models therefore allow to study the impact of separate transport sectors and to make sensitivity studies.

In a first step, the SCMs should be validated. Performing a limited set of dedicated experiments as well with the SCMs as with the AOGCMs could allow an interesting comparison between the behaviour of the SCMs and the AOGCMs. Two types of experiments which have a quite different impact on the atmosphere are chosen: changing the solar constant and changing the CO_2 concentration. Changing the solar constant affects the short-wave radiation and is felt mostly at the Earths surface; changing the CO_2 concentration affects the thermal infrared radiation and is initially felt mostly in the middle of the troposphere. The AOGCM experiments are performed with the Unified Model (UM) by the University of Reading, and with the CNRM-CM3 model by the CNRM. In a second step, the SCMs can be used to run a large set of climate simulations.

* *Corresponding author:* Dirk Olivié, Centre National de Recherches Météorologiques, 57 Avenue G. Coriolis, 31057 Toulouse, France. Email: dirk.olivie@cnrm.meteo.fr

The aim of this paper is to discuss the results from the climate scenario experiments obtained with the CNRM-CM3 model. Although these experiments are aimed to contribute to the validation of SCMs, the results of these experiments have also an intrinsic value. How differs the response to the solar forcing from the response to the CO_2 forcing? What is the response time of the model to these perturbations? What is the influence of the initial conditions on the response? Is the response time different for the ocean and the atmosphere?

This paper restricts itself mainly to the analysis of the time series of globally averaged annual mean values. In Section 2, we describe the experiments and the CNRM-CM3 model. In Section 3 we describe the results of the simulations, and in Section 4 we discuss the characteristics of the model response.

2 MODELS AND EXPERIMENTS

The CNRM-CM3 model is a global coupled climate model (Salas-Mélia et al., 2006). The system includes ARPEGE-Climat 3, which is the atmospheric part of the system (developed at CNRM), the OPA 8.1 ocean model (IPSL/LOCEAN, Paris, France), the GELATO-2 dynamic and thermodynamic sea ice model (CNRM) and the TRIP river routing scheme (University of Tokyo, Japan). These models are coupled together with OASIS2.2 (Terray et al., 1998). This software ensures that space interpolations between the different model grids and time synchronisation of the models are correct.

ARPEGE-Climat version 3 is fully described in Déqué et al. (1999) and Gibelin and Déqué (2003). The representation of most variables is spectral (T63 triangular truncation), while the physics are calculated on a 128 x 64 grid (about 2.8° resolution in longitude and latitude). This grid is reduced near the poles. The model contains 45 layers and the topmost layer is located at 0.05 hPa in order to correctly represent the atmospheric circulation in the stratosphere.

The OPA8.1 ocean model was developed by IPSL/LOCEAN (Paris, France) and is described in detail by Madec et al. (1998). It is used in its global configuration (182 x 152 points in the horizontal, without any North Pole singularity), i.e. about 2° resolution in longitude, while in latitude, its resolution varies from 0.5° at the equator to roughly 2° in polar regions. On the vertical, a z-coordinate is used (31 levels with 10 levels in the upper 100 m) is used.

The GELATO model was developed at CNRM and its second version is described in detail by Salas-Mélia (2002). The time step is 24 hours. GELATO-2 is a multi-category ice model (thickness dependant), and in CNRM-CM3, four categories were considered: 0-0.3m, 0.3-0.8m, 0.8-3m, and 3m or more.

The land surface scheme ISBA (Interactions Soil Biosphere Atmosphere) is used. The total runoff is converted into river discharge and transported to the ocean using the TRIP (Total Runoff Integrated Pathways) river routing system developed by T.Oki (Oki and Sud, 1998; Chapelon et al., 2002). The time step used in TRIP in the framework of CNRM-CM3 is 3 hours.

ARPEGE-Climat contains a parameterisation of the homogeneous and heterogeneous chemistry of ozone (Cariolle and Déqué, 1986; Cariolle et al., 1990).

A set of experiments (see Table 1) is performed with perturbations to CO_2 and the solar constant. They are represented by the letters C and S respectively. The perturbations consist in a sudden increase in CO_2 or the solar constant at time t_0 followed by an exponential decrease with a relaxation time τ_f of 2 or 20 year. The time evolution of $x(t)$ (which denotes either the CO_2 concentration or either the solar constant) can then be described by

$$\begin{aligned} x(t) &= x_b \quad \text{if} \quad t < t_0 \\ x(t) &= x_b + x_a \exp\left(-\frac{t-t_0}{\tau_f}\right) \quad \text{if} \quad t > t_0 \end{aligned} \tag{1}$$

where x_b = background value; and x_a = amplitude of the perturbation. The amplitude of the perturbations are chosen to give a comparable radiative forcing of around 10 Wm^{-2} at t_0. Therefore the solar constant was increased by 4.2 % (S20, S2 and S2b), and the pre-industrial CO_2 concentration of 286.2 ppmv was multiplied by a factor 6.5 (C20 and C2). In the experiment C2x where $\tau_f = \infty$

(which corresponds with a step forcing), the CO_2 concentration is only multiplied by two. The concentration of other green house gases (N_2O, CH_4, CFC's, …) are kept constant at their pre-industrial value. The initial conditions are taken from a reference simulation R performed with the same model under pre-industrial conditions. All simulations use the same initial conditions, except S2b. The CNRM-CM3 model is run for 100 year in C20 and S20, for 90 year in C2x, and for 50 year in C2, S2, and S2b.

We will show mainly the anomaly due to the perturbation, i.e. the difference between the simulations in Table1 and the reference simulation R.

Table 1 Overview of the different simulations.

Relaxation time (τ_f)	C (CO_2)	S (Solar)
20 year	C20	S20
2 year	C2	S2, S2b
∞	C2x	

3 RESULTS

3.1 *The atmosphere*

Time series of the anomaly in the surface (2m) air temperature are shown in Figure 1. For C20 and S20 (Fig.1, left panel) the response shows a strong increase in the first 5 year, a maximum between 5 and 15 year after t_0, and later a smooth decay. This smooth decay at the end is very similar to the shape of the forcing. The increase in the surface temperature is stronger in C20 than in S20. The responses of C2, S2 and S2b (Fig. 1, right panel) show a similar behaviour, although the maximum anomaly is much smaller, and the maximum is reached after 2 or 3 year. The initial increase is very short, and only a few data points during this increase are available. In accordance to C20 and S20, the anomaly in C2 is bigger than in S2 and S2b. The different initial conditions for S2 and S2b do not lead to a large difference: the maximum anomaly is very similar.

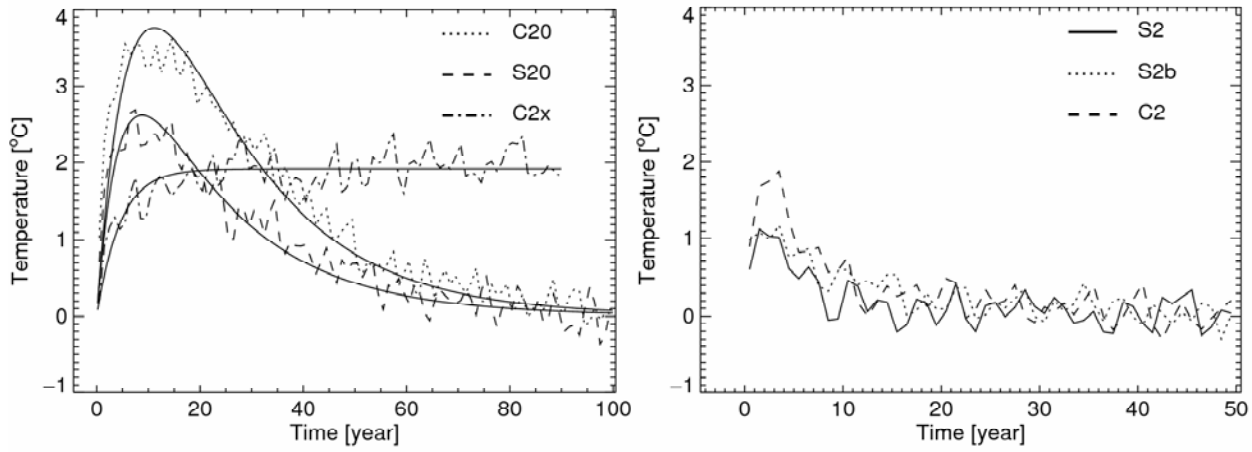

Figure 1: Anomaly of the surface (2m) air temperature. The left (right) panel gives the response when the relaxation time of the perturbation is 20 (2) year. Notice the different horizontal scale in the two panels.

Many other variables in the atmosphere (not shown) show a very similar behaviour as the surface (2m) air temperature. However, due to the disequilibrium at time t_0, there is also a fast response in C20 and C2: the liquid precipitation, the latent heat flux, and the top net long-wave radiation, show an immediate response which is opposite to the later response. Further, one finds a decrease in the cloud amount and an increase in the precipitation amount.

3.2 *The ocean*

Figure 2 shows the anomaly in the ocean temperature in C20 and S20. The maximum anomaly is reached after 40 to 50 year in C20, and after 35 year in S20. In a second phase, the ocean temperature anomaly decays in a regular way.

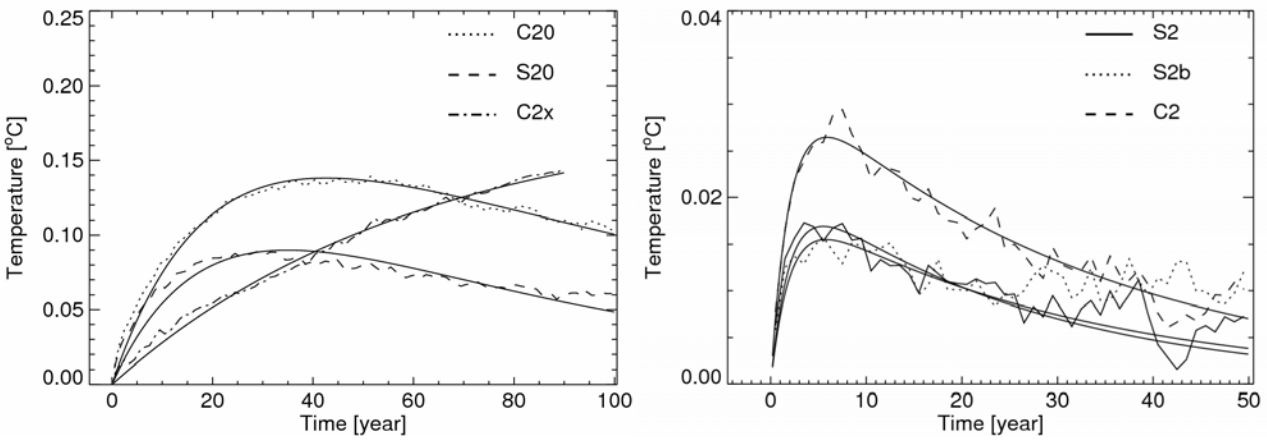

Figure 2: Anomaly of the ocean temperature for C20, S20 and C2x (left), and C2, S2, and S2b (right). Notice the different temperature scales.

Figure 3 shows the evolution of the vertical profile of the heat content anomaly in the ocean for C20. One clearly sees a maximum in the response at the depth of around 700 m after 50 to 60 year. At the surface there is a limited heating, during the first 20 year of the simulation. It takes a long time before the ocean actually starts heating. The heat is kept in a region below the mixed layer. In the last phase, one can also notice the start of the disappearance of the anomaly.

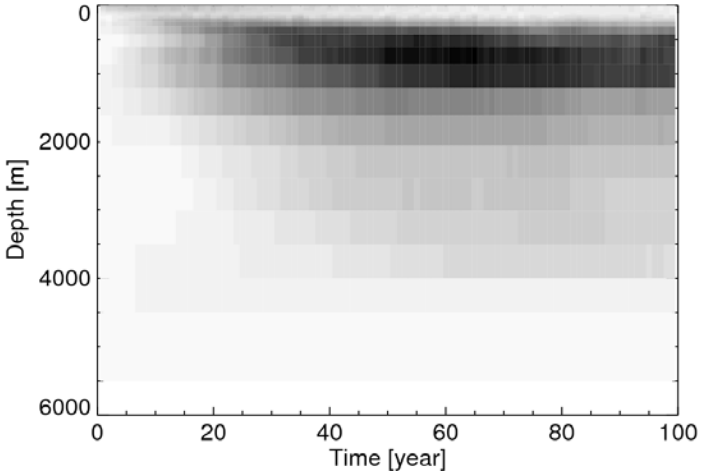

Figure 3: Profile of the ocean heat content anomaly in C20.

4 DISCUSSION

4.1 *Response time of the atmosphere and the ocean*

To study and interpret the time series, we use a simple model that describes rather well the response. The relation between the forcing *x(t)* and the response *y(t)* of this simple mode is

$$\frac{dy}{dt} + \frac{y}{\tau_s} = f\,x \tag{2}$$

where f = sensitivity; and τ_s = response time. If the forcing is given by Equation 1, then the solution of Equation 2 is described by

$$y(t) = 0 \quad \text{if} \quad t < t_0$$

$$y(t) = \frac{f\,x_a}{\frac{1}{\tau_s} - \frac{1}{\tau_f}} \left(\exp\left(-\frac{t - t_0}{\tau_f} \right) - \exp\left(-\frac{t - t_0}{\tau_s} \right) \right) \quad \text{if} \quad t > t_0 \tag{3}$$

This simple model allows us to derive the response time τ_s of the system. By fitting the curve suggested in Equation 3 through the observed time series, we find that the response time of the atmosphere derived from C20 and S20 lies for many variables between 5 and 10 year. The results from the curve-fitting are also indicated in Figures 1 and 2.

Table 2 gives the response time of the mean ocean temperature, derived in the different experiments. From the C20 and S20 experiments, a relaxation time of respectively 117 and 70 year has been derived. C2, S2 and S2b all give a relaxation time around 30 year. Apparently there is a strong difference depending on the relaxation time of the forcing. The results from C2, S2 and S2b should be taken with care, because the values in the time series of the anomalies fluctuate very strongly. Therefore we have for C2, S2 and S2b only used the first 25 year of the time series to do the curve fitting.

Table 2: Response time of the ocean temperature.

Experiment	Relaxation time (year)
C20	117
S20	70
C2	32
C2x	61
S2	25
S2b	30

In general, the response time of the ocean should be taken with care. In the reference simulation R, the ocean temperature shows a linear decrease of -0.08 °C / century. This trend has to be compared with the observed decreases in the model simulations and might complicate the interpretation of the ocean relaxation time.

4.2 *Influence of the initial conditions*

Concerning the influence of the initial conditions, Table 3 gives for a selection of atmospheric variables the maximum anomaly for the S2 and S2b simulations. These two simulations have the same forcings but different initial conditions. The values for most variables differ not more than 10 to 20 %, and their difference is often significantly smaller than the inter-annual variability (Table 3, last column). Only the anomaly in the high cloud amount seems to be quite different in the two simulations.

Table 3: Maximum anomaly for different variables in S2 and S2b. The last column shows the inter-annual variability in the reference experiment R.

		S2	S2b	R (inter-annual variability)
Surface (2m) air temperature	°C	1.12	1.17	0.17
Liquid precipitation	mm day^{-1}	0.089	0.114	0.018
Solid precipitation	mm day^{-1}	-0.0091	-0.011	0.0030
Total cloud amount	%	-0.85	-0.84	0.27
Low cloud amount	%	-0.86	-0.92	0.34
Medium cloud amount	%	-1.04	-1.06	0.21
High cloud amount	%	-0.45	-0.92	0.21
Surface latent heat flux	W m^{-2}	0.85	0.97	0.44
Surface sensible heat flux	W m^{-2}	-0.18	-0.17	0.14
Sea surface temperature	°C	0.88	0.84	0.13

For the ocean temperature (Fig. 2, right panel), one can see that the initial conditions have a very small effect on the maximum anomaly.

4.3 *Comparison with other experiments*

With the CNRM-CM3 model many other experiments have been performed. Two interesting experiments are simulations where the CO_2 concentration is increased gradually by 1 % per year till a doubling (Cg2) or a quadrupling (Cg4) is reached, after which the concentration is kept constant (Figure 4, left panel). The surface (2m) air temperature from the pulse experiment C20 and from

these experiments is compared. If one assumes that the response of the model to some forcing is linear, the response to an arbitrary forcing *x(t)* can be found by convoluting this arbitrary forcing with the response of the pulse experiment

$$y(t) = \frac{H}{x_a} \otimes \left(\frac{x}{\tau_f} + x' \right) = \int_0^t \frac{H(t-t')}{x_a} \left(\frac{x(t')}{\tau_f} + x'(t') \right) dt' \qquad (4)$$

where *H(t)* = the response to the pulse perturbation. In the right panel of Figure 4, the response of the different experiments C20, R, Cg2 and Cg4 is indicated, together with the result of the convolution. For Cg2 the correspondence between the convolution and the real simulation is rather good, although the trend on the long term is lacking. For Cg4, the convolution gives much higher values than the real simulation, due to the fact that the perturbation experiment is seen as a perturbation in the CO_2 concentration, and not in the logarithm of the CO_2 concentration. Assuming a linear relation between the temperature change and the logarithm of the CO_2 concentration, one finds results which for the Cg4 simulation agree much better.

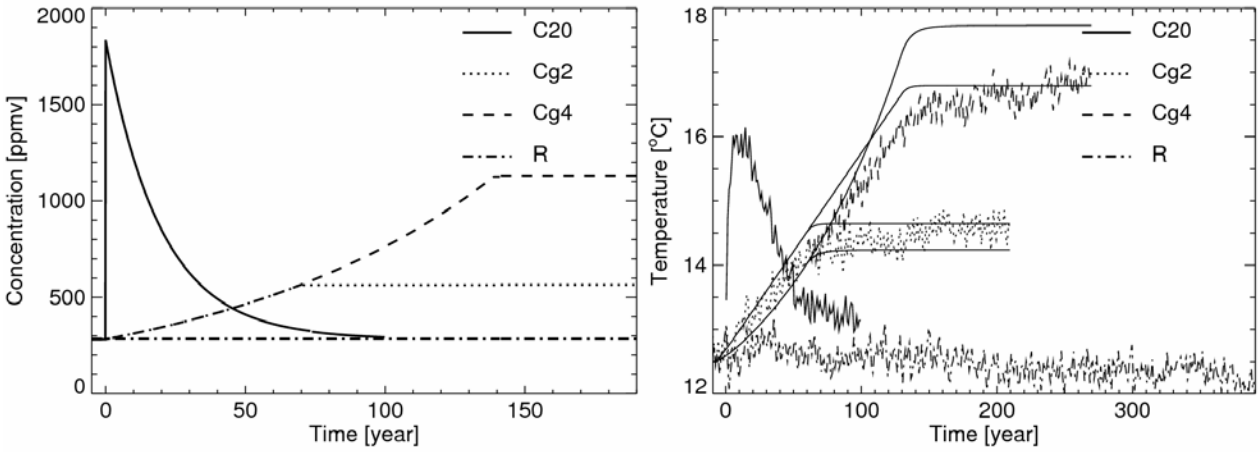

Figure 4: Left: different scenarios for the CO_2 concentration. Right: surface (2m) air temperature response in C20, C2g, and Cg4. The straight lines are the results of the convolution

REFERENCES

Cariolle, D. and M. Déqué, 1986. Southern hemisphere medium-scale waves and total ozone disturbances in a spectral general circulation model. *J. Geophys. Res 91*, 10825-10846.

Cariolle, D., A. Lasserre-Bigory, J.-F. Royer and J.-F. Geleyn, 1990. A general circulation model simulation of the springtime Antarctic ozone decrease and its impact on mid-latitudes. *J. Geophys. Res. Atmos. 95*, 1883-1898.

Chapelon, N., H. Douville, P. Kosuth and T. Oki, 2002. Off-line simulations of the Amazon water balance: a sensitivity study with implications for GSWP, *Climate Dynamics 19*, 141-154.

Déqué, M., A. Braun, J.-P. Piedelievre, P. Marquet, P. Dandin, J.-F. Guérémy, J.-F. Geleyn, E. Bazile, J.-M. Piriou, K. Yessad, P. Courtier and P. Rochas, 1999. *ARPEGE version 3, documentation algorithmique et mode d'emploi*, Météo-France, CNRM/GMEGEC, Toulouse 31057, France.

Gibelin, A.-L. and M. Déqué, 2003. Anthropogenic climate change over the Mediterranean region simulated by a global variable resolution model. *Climate Dynamics 20*, 327-339.

Madec, G., P. Delecluse, M. Imbard and C. Lévy, 1998. *OPA version 8.1 Ocean General Circulation Model Reference Manual*. Notes du Pôle de Modélisation No. 11, Institut Pierre-Simon Laplace, Université Paris VI, Laboratoire d'Océanographie Dynamique et de Climatologie, Paris 75252, France, 91 pp.

Oki, T. and Y. C. Sud, 1998. Design of total runoff integrating pathways (TRIP) A global river channel network. *Earth Interactions*, vol. 2, paper 1.

Salas-Mélia, D., 2002. A global coupled sea-ice ocean model. *Ocean Modelling 4*, 137-172.

Salas-Mélia, D., F. Chauvin, M. Déqué, H. Douville, J. F. Guérémy, P. Marquet, S. Planton, J.-F. Royer and S. Tyteca, 2006. Description and validation of the CNRM-CM3 global coupled model. Submitted to *Climate Dynamics*.

Terray, L., S. Valcke and A. Piacentini, 1998. OASIS 2.2 User's Guide and Reference Manual. TR/CMGC/98-05, CERFACS, Toulouse, France.

Quantifying the effects of aviation on radiative forcing and temperature with a climate response model

L. Lim*, D.S. Lee,
Dalton Research Institute, Department of Environmental & Geographical Sciences, Manchester Metropolitan University, UK

R. Sausen, M. Ponater
Space and Atmospheric Research Group, Imperial College London, UK

Keywords: Climate response, aviation, efficacy

ABSTRACT: Simplified climate models can be used to calculate and to compare temperature response contributions from small forcings without the need for considerable computer resources. A linear climate response model using Green's functions has been formulated to calculate radiative forcing (RF) and the global mean temperature response from aviation. The model, LinClim, can calculate aviation RF for CO_2, O_3, CH_4, water vapour, contrails, sulphate and black carbon aerosols. From these RFs, temperature responses may be calculated for individual effects in order to determine their relative importance by applying preliminary values for efficacies. The LinClim model is tuned to reproduce the dominant mode of its parent coupled atmosphere-ocean GCM, ECHAM4/OPYC3. LinClim is able to reproduce the IPCC (1999) 2050 aviation-related forcings. The model is shown through some example application analyses to be a useful tool for exploring the effects of aviation on RF and temperature response.

1 INTRODUCTION

Aircraft emissions may influence climate from a number of emissions and effects. These effects have been reviewed and assessed in the Intergovernmental Panel on Climate Change (IPCC) Special Report '*Aviation and the Global Atmosphere*' (IPCC, 1999). More recently, Sausen et al., (2005) gave an update to the IPCC results on the aviation's impact on climate by means of the metric 'radiative forcing of climate'. This metric has been adopted by the IPCC (IPCC, 1990) and the scientific community to assess different anthropogenic effects on climate. The RF concept has proven useful as there is an approximately linear relationship between the global mean radiative forcing (*RF*) and the associated equilibrium global mean surface temperature change (ΔT_s), i.e.:

$$\Delta T_s \approx \lambda \, RF \ , \qquad (1)$$

where λ is the climate sensitivity parameter (unit K/Wm^{-2}). For many years λ has been considered being a model constant, independent of the type of forcing. More recently, in a number of studies, it has been shown that λ is to some extent also dependent on the type of perturbation, in particular for non-homogeneously distributed climate change agents, e.g., aircraft-induced O_3 perturbations (Hansen et al., 1997; Forster and Shine, 1997; Ponater et al., 1999; Joshi et al., 2003). This is sometimes denoted the 'efficacy' (Hansen et al., 2005) and is defined as:

$$r_i = \lambda_i / \lambda_{CO2} \ , \qquad (2)$$

where λ_i and λ_{CO2} are the climate sensitivity parameters associated with perturbations of the climate change agent *i* and of CO_2, respectively. Considering also the efficacy, eq. (1) modifies to

$$\Delta T_s \approx r_i \lambda_{CO2} RF \ . \qquad (3)$$

* *Corresponding author:* Ling Lim, Dalton Research Institute-CATE, Manchester Metropolitan University, Faculty of Science and Engineering, John Dalton East Building, Chester St, Manchester M1 5GD, UK. Email: l.lim@mmu.ac.uk

The ideal way to explore climate scenarios would be to perform simulations with general circulation models (GCMs). However, GCMs are very complex and computationally demanding: a scenario may need to be run (depending on the climate perturbation) for decades of simulation time taking processing time in the order of weeks to months on a high performance computer (in particular if chemistry is included). The necessity for long simulation periods arises from climate inertia effects and the requirement to separate signal from noise. For aircraft perturbations that are relatively small, this is a particularly difficult problem. In order to overcome the high computational costs associated with determining environmental responses with GCMs, simplified climate response models may be used. Such models are generally tuned or parameterized to reproduce the main characteristic responses of GCMs (such as the temporal evolution of the global mean near surface temperature) and have been used extensively by the IPCC to explore the impacts of a large range of climate scenarios (IPCC, 2001).

Sausen and Schumann (2000) (hereafter referred to as S&S 2000) demonstrated that some of the global mean environmental responses to particular engine technology development scenarios could be conveniently explored with a simple linear climate response model that was computationally efficient. This model went beyond RFs to compute temperature responses over various timescales. Using temperature response rather than RF allows an examination of the effects of r_i by looking at the time-development of changes in ΔT_s, and an assessment of the relative merits of abatement technologies in terms of climate protection.

In this paper, a simplified climate response model, LinClim, which builds upon the approach of S&S (2000) is presented. The scope of the model has been expanded to include the full suite of aviation-specific effects identified by the IPCC (1999). These include RFs and temperature response formulations for CO_2, formation of O_3 and CH_4 destruction due to NO_x, water vapour, contrails, sulphate, soot and indirect clouds.

2 MODEL DESCRIPTION

The modelling approach adopted was to calculate the emissions and subsequent concentrations of a climate gas, calculate its RF, and then to calculate the ΔT_s due to the RF using a simplified climate response function. LinClim includes formulations which are consistent with either the IPCC (1999) or TRADEOFF (Sausen et al., 2005) data (denoted '*99*' and '*TO*', respectively). For methodologies that involves reference year scaling, the values may be obtained from various sources.

2.1 *Carbon dioxide (CO_2)*

In order to calculate the full CO_2 contribution to RF and temperature response, historical fuel and extrapolation out to 2100 were calculated using S&S (2000) methodology. Emissions of CO_2 are then calculated using carbon mass fraction of 0.86 for aviation fuel (S&S 2000). The response of CO_2 concentrations to an emissions rate is modelled using Hasselmann et al., (1997), which approximates to the results of the carbon cycle model of Maier-Reimer and Hasselmann (1987).

The RF of a CO_2 increase is dependent upon the reference concentration because of spectral saturation, such that in calculating the impacts of CO_2 from aviation, it is necessary to know the 'background' RF. Historical CO_2 concentration data from 1800 until 1995, and thereafter until 2100 from IPCC scenario IS92a (all natural and anthropogenic sources including aircraft emissions) were used as background (S&S 2000). The contribution of aviation CO_2 concentrations are calculated explicitly, the concentration being assumed to be the difference between background and aviation concentrations. The RF of CO_2 may then be calculated using the simplified expression adopted by IPCC (1997) or IPCC (2001).

2.2 *NO_x-induced ozone (O_3) and methane (CH_4)*

The aviation O_3 and CH_4 RF methodology assumes that there is a linear relationship between aviation NO_x emissions and O_3 (and indirect CH_4) RF changes (IPCC, 1999), i.e.:

$$RF_{O3,CH4}(t) = RF_{O3,CH4}(ref\ year) \times \frac{E_a(t)}{E_a(ref\ year)} \times \frac{EI_{NOx}(t)}{EI_{NOx}(ref\ year)}\ , \qquad (4)$$

where E_a is the aircraft fuel burnt per year, and EI_{NOx} is the emissions index of nitrogen oxides per mass of fuel burnt.

2.3 *Water vapour (H_2O)*

Similar to the calculation of aviation induced O_3 and CH_4, a simplified linear approach is taken for water vapour where the RF scales linearly with fuel use, i.e.:

$$RF_{H2O}(t) = RF_{H2O}(ref\ year) \times \frac{E_a(t)}{E_a(ref\ year)}\ , \tag{5}$$

2.4 *Line-shaped contrails*

Contrails RF is assumed to scale with fuel burn and an additional factor, F, to account for the evolution of fleet and flight routes over time (IPCC, 1999) and F was then derived by scaling this RF value to the published values in IPCC (1999) for the years 2015 and 2050. Post 2050, F is assumed to be constant. The F values are summarized in Table 1.

Table 1: Correction factor, F to account for fleet evolution and flight routes

Year	Technology 1	Technology 2
1992	1.00	1.00
2015	1.48	1.48
2050	1.70	1.64

2.5 *Sulphate (SO_4) and soot (BC) particles*

Aviation SO_4 particle emissions were derived from the sulphur content of fuel, as in eq. (6), where $E_{SO4}(t)$ is the aviation emissions at time t (Tg S), $EI_{Sulphur}$ is the emissions index 0.0004 kg S per kg fuel, β is the effective conversion factor from fuel-sulphur to optically active sulphate, following IPCC (1999), we adopt β = 50%.

$$E_{SO4}(t) = \beta \times EI_{Sulphur} \times E_a(t) \tag{6}$$

Aviation soot (black carbon, BC) is calculated using eq. (7), where $E_{BC}(t)$ is the aviation emissions at time t (Tg BC) and EI_{BC} is the emissions index 0.00004 kg black carbon per kg fuel (IPCC, 1999).

$$E_{BC}(t) = EI_{BC} \times E_a(t) \tag{7}$$

RF for particles is scaled to the respective particle emissions and externally calculated RF.

$$RF_{SO4,BC}(t) = RF_{SO4,BC}(ref\ year) \times \frac{E_{SO4,BC}(t)}{E_{SO4,BC}(ref\ year)} \tag{8}$$

2.6 *Aviation-induced cirrus*

Similar to the water vapour RF calculation, it is assumed that RF of aviation-induced cirrus scales with fuel usage. However, due to the large uncertainties in aviation-induced cirrus calculation (c.f., Sausen et al., 2005; or Mannstein and Schumann, 2007), we refrain from including the contribution from this effect in the final results.

2.7 *Temperature response*

The temperature response approach was devised by Hasselmann et al., (1993) and has been widely used thereafter (e.g., Hasselmann et al., 1997; S&S 2000). The formulation presented by S&S (2000) has been rearranged to include the perturbation's efficacy:

$$\Delta T_i(t) = r_i \lambda_{CO2} \int_0^t \hat{G}_T(t-t')\, RF_i(t')\, dt'\ , \tag{9}$$

$$\hat{G}_T(t) = \frac{1}{\tau} e^{-t/\tau}\ , \tag{10}$$

where ΔT_i is the temperature response (K) due to perturbation *i*. r_i is the associated efficacy, λ_{CO2} is the CO_2 climate sensitivity parameter (K/Wm^{-2}) of the parent GCM, RF_i is the associated radiative forcing (Wm^{-2}). The revised Green's function is $\hat{G}_T(t)$, τ is the lifetime (e-folding time) of a temperature perturbation (years). The current version of LinClim is tuned to reproduce the transient behaviour of the full-scale atmosphere ocean model ECHAM4/OPYC3 (Roeckner et al., 1999). The value of λ_{CO2} is 0.64 K/Wm^{-2} and τ is 37.4 years. The values for r_i are summarized in Table 2.

Table 2: Efficacies, r_i

Perturbation	Reference	r_i (range)
CO_2, SO_4, BC		1
Aviation O_3	Ponater et al., 2006	1.37 (1 – 2)
CH_4	Ponater et al., 2006	1.18 (1 – 1.2)
H_2O	Ponater et al., 2006	1.14
Contrails	Ponater et al., 2006	0.59

3 APPLICATION

The aviation RF results from LinClim using the '*99'* parameters (scaled to IPCC (1999) reference values parameters summarized in Table 3), denoted as LC-99, are presented in Table 4. The IPCC (1999) results are basically reproduced. The deviations in RF_{CO2} result from a slightly different CO_2 concentration. There were noticeable differences in the 1992 RF_{O3} and $RF_{Contrails}$. This is due to the difference in the 1992 fuel burnt in LinClim (165.1 Tg from S&S, 2000) and the IPCC (1999) (160.3 Tg). Small differences were yielded also for RF_{O3} and RF_{CH4} in future years. This is because the IPCC (1999) RF_{O3} and RF_{CH4} results were obtained from CTM runs, whereas the results from LC-99 were simply scaled to the NO_x emissions.

Table 3: Reference year (1992 and 2000) parameters used in the example applications

Parameter	Unit	Reference values in 1992 (used in LC-99)	Reference values in 2000 (used in LC-TO)
E_a	Tg/Yr	160.3*	169.0†
E_{SO4}	Tg S	0.032*	0.0338‡
E_{BC}	Tg BC	0.006*	0.0068‡
EI NO_x	g NO_2/kg fuel	12.0*	12.7†
RF_{O3}	W/m^2	0.023*	0.0219‡
RF_{CH4}	W/m^2	-0.014*	-0.0104‡
RF_{H2O}	W/m^2	0.0015*	0.0020‡
$RF_{Contrails}$	W/m^2	0.020*	0.0100‡
RF_{SO4}	W/m^2	-0.003*	-0.0035‡
RF_{BC}	W/m^2	0.003*	0.0025‡

*IPCC (1999), †Gauss et al. (2006), ‡Sausen et al. (2005).

A second set of parameters from the TRADEOFF study (Sausen et al., 2005) were used to form an updated version of LinClim, denoted as LC-TO (Table 3). These updated results (see Table 4) show that the contribution of aviation RF is lower than in the previous assessments, both for 1992 and for future scenarios.

Figure 1 shows the total aviation RF (without aviation-induced cirrus) and the associated temperature changes (with and without considering the efficacies) for scenario Fa1 calculated using LinClim with the TRADEOFF parameters (LC-TO). It is interesting to note the role of efficacies in the temperature prediction. Using an efficacy of 1 for all perturbations, the temperature response is approximately the same as the prediction including individual efficacy values for specific perturbation (as listed in Table 2). By chance, the larger contributions from O_3 and H_2O are offset by the smaller contribution from contrails and the more negative contribution from CH_4. However, by changing the efficacy of O_3 to the lower (r_{O3} = 1) and upper (r_{O3} = 2) bounds, the temperature response is 20% lower (r_{O3} = 1) or 33% higher (r_{O3} = 2) than the case where r_{O3} = 1.37 (as in Table 2) at 2100. This shows that the role of efficacies may become increasingly important in determining

the tradeoffs between different engine technology options, in particular with respect to NO_x which causes component impacts of high efficacy.

Table 4: RF comparison of LinClim with the IPCC (1999) parameters (LC-99) and with the TRADEOFF parameters (LC-TO). (Cont. = Contrails)

Scenario	Data source	CO_2 (ppmv)	Radiative forcing (W/m2) CO_2	O_3	CH_4	H_2O	Cont.	SO_4	BC	Total
NASA-1992	IPCC	1.0	0.018	0.023	-0.014	0.002	0.020	-0.003	0.003	0.049
	LC-99	1.3	0.022	0.024	-0.014	0.002	0.021	-0.003	0.003	0.054
	LC-TO	1.3	0.019	0.020	-0.012	0.002	0.010	-0.003	0.002	0.038
NASA-2015	IPCC	2.5	0.038	0.040	-0.027	0.003	0.060	-0.006	0.006	0.114
	LC-99	2.8	0.044	0.052	-0.032	0.003	0.060	-0.006	0.006	0.128
	LC-TO	2.8	0.038	0.044	-0.025	0.004	0.028	-0.007	0.005	0.087
FESGa (tech1) 2050	IPCC	6.0	0.074	0.060	-0.045	0.004	0.100	-0.009	0.009	0.193
	LC-99	6.3	0.080	0.086	-0.052	0.004	0.100	-0.009	0.009	0.218
	LC-TO	6.3	0.068	0.073	-0.044	0.006	0.047	-0.010	0.007	0.147
FESGa (tech2) 2050	IPCC	6.1	0.075	0.047	-0.035	0.005	0.100	-0.009	0.009	0.192
	LC-99	6.4	0.081	0.066	-0.040	0.005	0.100	-0.009	0.009	0.212
	LC-TO	6.4	0.069	0.057	-0.027	0.006	0.047	-0.010	0.007	0.149

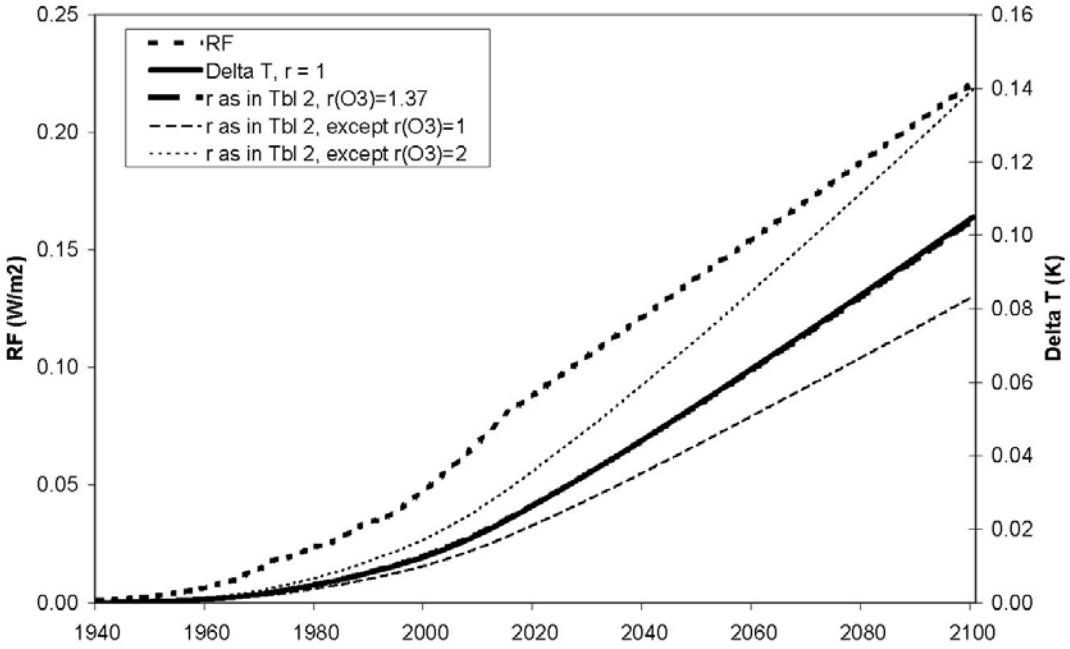

Figure 1: Aviation RF and associated temperature changes (with and without considering the efficacies) for scenario Fa1

4 CONCLUSIONS AND FURTHER WORK

The RF and temperature response results of the simple climate response model, LinClim, are presented. LinClim is able to predict the temperature response from the full suite of aviation perturbations. The present day and future scenario RF results compared well with the published IPCC (1999) values. LinClim's RF results are not intended to replace other RF estimates, but are rather used to describe the contribution of individual impact components to the total aviation effect for transient emission scenarios. In future work the model will be applied more extensively to various technology and growth scenarios to understand the role of aviation and by how technology im-

provements may be best targeted. Moreover, the model will also be useful in exploring more appropriate climate metrics than RF for policy applications.

5 ACKNOWLEDGEMENTS

This study was funded by the EU IP QUANTIFY and EU NoE ECATS. Further support was given from the UK Department of Trade and Industry (DTI) and the UK Department for Transport (DfT).

REFERENCES

Forster, P.M.D. and K.P. Shine, 1997: Radiative forcing and temperature trends from stratospheric ozone changes. *J. Geophy. Res. 102*, 10841–10855.

Gauss, M., I.S.A. Isaksen, D.S. Lee and O.A. Søvde, 2006: Impact of aircraft NO_x emissions on the atmosphere – tradeoffs to reduce the impact. *Atmos. Chem. Phys. 6*, 1529–1548.

Hansen, J.E., M. Sato and R. Ruedy, 1997: Radiative forcing and climate response. *J. Geophy. Res. 102*, 6831–6684.

Hansen, J., M. Sato, R. Ruedy, L. Nazarenko, A. Lacis, G.A. Schmidt, G. Russell and 38 other co-authors, 2005: Efficacy of climate forcings. *J. Geophy. Res. 110*, D18104, doi:10.1029/2005JD005776.

Hasselmann, K., R. Sausen, E. Maier-Reimer and R. Voss, 1993: On the cold start problem in transient simulations with coupled atmosphere-ocean models. *Clim. Dyn. 9*, 53–61.

Hasselmann, K., S. Hasselmann, R. Giering, V. Ocana and H. von Storch, 1997: Sensitivity study of optimal CO_2 emission paths using a Simplified Structural Integrated Assessment Model (SIAM). *Clim. Change 37*, 345–386.

IPCC, 1990: *Climate Change: The IPCC Scientific Assessment*. Contribution of Working Group I to the First Assessment Report of the Intergovernmental Panel on Climate Change. J.T. Houghton, G.J. Jenkins and J.J. Ephraums (eds). Intergovernmental Panel on Climate Change, Cambridge University Press, UK.

IPCC, 1997: *An introduction to simple climate models used in the IPCC Second Assessment Report*. IPCC Technical Paper II. J.T. Houghton, L. Gylvan Meira Filho, D.J. Griggs and K. Maskell (eds), Intergovernmental Panel on Climate Change, Switzerland.

IPCC, 1999: *Aviation and the Global Atmosphere*. A Special Report of IPCC Working Groups I and III in collaboration with the Scientific Assessment panel to the Montreal Protocol on Substances that Deplete the Ozone Layer. J.E. Penner, D.H. Lister, D.J. Griggs, D.J. Dokken and M. McFarland (eds). Intergovernmental Panel on Climate Change, Cambridge University Press, UK.

IPCC, 2001: *Climate Change 2001: The Scientific Basis*. Contribution of Working Group I to the Third Assessment Report of the Intergovernmental Panel on Climate Change. J.T. Houghton, Y. Ding, D.J. Griggs, M. Noguer, P.J. van der Linden, X. Dai, K. Maskell and C.A. Johnson (eds). Intergovernmental Panel on Climate Change, Cambridge University Press, UK.

Joshi, M., K. Shine, M. Ponater, N. Stuber, R. Sausen and L. Li, 2003: A comparison of climate response to different radiative forcings in three general circulation models: towards an improved metric of climate change. *Clim. Dyn. 20*, 843–854.

Maier-Reimer, E. and K. Hasselmann, 1987: Transport and storage of CO_2 in the ocean – An inorganic ocean-circulation carbon cycle model. *Clim. Dyn. 2*, 63–90.

Mannstein, H. and U. Schumann, 2007: Corrigendum to "Mannstein, H., U. Schumann, 2005: Aircraft induced contrails over Europe. Meteorol. Zeit. 14, no. 4, p. 549–554.", *Meteorol. Zeit.*, in press.

Ponater, M., R. Sausen, B. Feneberg and E. Roeckner, 1999: Climate effect of ozone changes caused by present and future air traffic. *Clim. Dyn. 15*, 631–642.

Ponater, M., S. Pechtl, R. Sausen, U. Schumann and G. Hüttig, 2006: Potential of the cryoplane technology to reduce aircraft climate impact: A state-of-the-art assessment. *Atmos. Environ. 40*, 6928-6944.

Roeckner, E., L. Bengtsson, J. Feichter, J. Lelieveld and H. Rodhe, 1999: Transient climate change simulations with a coupled atmosphere-ocean GCM including the tropospheric sulfur cycle. *J. Climate 12*, 3004-3032.

Sausen, R. and U. Schumann, 2000: Estimates of the climate response to aircraft CO_2 and NO_x emissions scenarios. *Clim. Change 44*, 27–58.

Sausen, R., I. Isaksen, V. Grewe, D. Hauglustaine, D.S. Lee, G. Myhre, M.O. Köhler, G. Pitari, U. Schumann, F. Stordal and C. Zerefos, 2005: Aviation radiative forcing in 2000: an update on IPCC (1999). *Meteorol. Zeit. 114*, 555–561.

Radiative forcing and temperature response from shipping

D. S. Lee*, L. Lim
Dalton Research Institute, Manchester Metropolitan University, John Dalton Building, Chester Street, Manchester M1 5GD, United Kingdom

V. Eyring, R. Sausen
DLR-Institut für Physik der Atmosphäre Oberpfaffenhofen, Germany

Ø. Endresen, H.-L. Behrens
Det Norske Veritas, Veritasveien1, N-1322 Høvik, Norway

Keywords: Radiative forcing, simple climate model, shipping emissions, temperature response

ABSTRACT: A simplified global climate response model was used to calculate radiative forcings and temperature responses from the emissions of shipping. Radiative forcings were calculated for 2000, which were: 0.043 W m^{-2} (CO_2); 0.021 W m^{-2} (O_3); -0.011 W m^{-2} (CH_4). If these forcings are combined with literature values for SO_4, black carbon and the indirect aerosol effect, a total forcing of -0.08 W m^{-2} was calculated. Comparing the 2000 CO_2 shipping radiative forcing and temperature responses with those for aviation showed them to be approximately 1.8× and 2.7× greater.

1 INTRODUCTION

Ocean-going shipping provides an important means of international transportation of goods, along with other purposes such as fishing, leisure transport etc. Shipping has been operational on an international scale since approximately the industrial revolution, initially as sail ships, then steam ships powered by coal. Since *circa* 1910, diesel engines were introduced. By 1961, there were still over 10,000 steam engine powered ships and ~3,500 steam turbine powered ships in operation.

The combustion of coal and diesel results in a variety of emissions including carbon dioxide (CO_2), oxides of nitrogen (NO_x), carbon monoxide (CO), methane (CH_4), other non-methane volatile organic compounds (VOCs) and particles. In addition to sulphate particles (SO_4) resulting from SO_2 emissions, ships also release black carbon (BC) and particulate organic matter (POM).

These emissions contribute to perturbation of the global carbon, sulphur and nitrogen budgets. They result in both direct warming effects from CO_2 and CH_4, potential indirect warming effects from the emission of ozone (O_3) precursors (NO_x, CH_4, CO and VOCs) and indirect cooling effects from shipping emissions of NO_x, which increases OH resulting in a reduction in CH_4 lifetime (Endresen et al., 2003; Eyring et al., 2007). The increases in SO_4 and BC concentrations also have direct but opposing effects resulting from enhanced scattering and reflection of solar radiation/downwelling of long-wave radiation and an indirect effect from the formation of 'ship tracks' (e.g. Schreier et al., 2006) and large-scale low marine clouds (Capaldo et al., 1999).

In this work, the global mean radiative forcing (RF) and temperature response from shipping emissions was calculated for most of the forcing agents. A climate response model was adapted to deal with shipping radiative effects in a parameterized way from a similar model developed for evaluating global mean aviation effects (Lim et al., 2007), which in turn was developed from the simpler model of Sausen and Schumann (2000). Such climate response modelling was originally developed by Hasselmann et al. (1993), which has been adapted for a variety of applications.

Since much research has been dedicated to understanding the response of the climate system to aircraft emissions, some simple comparisons are made between the two transportation sectors and projected emissions scenarios in the future.

* *Corresponding author:* D. S. Lee, Dalton Research Institute-CATE, Manchester Metropolitan University, Faculty of Science and Engineering, John Dalton East Building, Chester St, Manchester M1 5GD, UK. Email: D.S.Lee@mmu.ac.uk

2 METHODOLOGY

In this section, the emissions estimations are summarized and details of the climate response model provided that are particular to the quantification of shipping RF and temperature responses.

2.1 *Emissions*

Present day shipping emissions are taken from Eyring et al. (2005a; hereafter EY2005a) for CO_2, NO_x, VOCs, CH_4 and CO. Historical emissions from shipping were taken from two different sources for comparison. EY2005a calculated emissions from 1950 to 2001. However, engine-driven shipping has a much longer history that dates back to *circa* 1870. For earlier shipping emissions, shipping emissions data are taken from Endresen et al. (2007). Two estimations of shipping CO_2 radiative forcing can be made to 2000; one using the data of Endresen et al. (2007; hereafter EN2007) and another using these data from 1870 to 1950 combined with EY2005a from 1950 to 2000.

For future emissions, Eyring et al. (2005b) provided estimations according to four demand scenarios (DS1-DS4) and four technology scenarios (TS1-TS4) to 2050. However, in order to better represent the climate response, transient runs to 2100 are needed. Therefore, the central demand/technology scenario (DS1-TS4) of Eyring et al. (2005b) has been extrapolated out to 2100.

For the comparison with aviation, a full historical and projected scenario of emissions from 1940 through to 2050, extrapolated out until 2100 has been taken from Sausen and Schumann (2000).

2.2 *Climate response model*

The LinClim climate response model (Lim et al., 2007) has been adapted to calculate RFs and temperature responses from shipping emissions. The contribution of shipping emissions of CO_2 to concentrations was calculated according to the method of Hasselmann et al. (1997) and these were subtracted from historical 'background' CO_2 concentrations up until 1995, thereafter using concentrations from the IS92a scenario to 2100. The CO_2 RF was then calculated from the CO_2 concentrations according to the method of IPCC (2001). The temperature response was calculated via a convolution integral method (Hasselmann et al., 1993) using an updated fit to the parent GCM, ECHAM4/OPYC3 (Lim et al., 2007).

For CH_4, a global mean mass balance equation was used, which accounts for changes in CH_4 lifetime from tropospheric, stratospheric and soil sinks (Wigley et al., 2002). The tropospheric lifetime, τ_{OH}, was determined from Equation [1] (IPCC, 2001).

$$\delta \ln(\tau_{OH})_t = -0.32\delta \ln(C)_{t-1} + 0.0042\delta(e-NO_X)_t - 0.000105\delta(e-CO)_t - 0.000315\delta(e-VOC)_t \quad [1]$$

where $(\tau_{OH})_t$ is the tropospheric sink at time t (yr), $(e\text{-}NO_x)_t$ are the anthropogenic NO_x emissions at time t (Tg(N)/yr), $(e\text{-}CO)_t$ are the anthropogenic CO emissions at time t (Tg/yr), and $(e\text{-}VOC)_t$ are the anthropogenic VOC emissions at time t (Tg/yr)

It was assumed that all changes in lifetime, concentration and emissions are relative to the year 2001. It was also assumed that the natural emissions of CH_4, NO_x, CO and VOC remain constant. The mass balance equation predicts background CH_4 and the same equation was used to calculate the shipping component, using the difference between background and shipping emissions of NO_x, CO, CH_4 and VOCs in Equation [1].

The RF arising from the CH_4 perturbation was calculated from the method presented by IPCC (2001) which accounts for N_2O overlap.

$$RF_{CH_4} = \alpha\left(\sqrt{C_{(t)}} - \sqrt{C_0}\right) - \left(f(C_t, N_0) - f(C_0, N_0)\right) \quad [2]$$

where α is 0.036, C_t is the CH_4 concentration at time t (ppbv), C_0 is the pre-industrial CH_4 concentration (700 ppbv), N_0 is the pre-industrial N_2O concentration (280 ppbv) and $f(C,N)$ is the correction for overlap with N_2O:

$$f(C,N) = 0.47 \ln\left(1 + 2.01\times10^{-5}(C\cdot N)^{0.75} + 5.31\times10^{-15}C(C\cdot N)^{1.52}\right) \quad [3]$$

The CH_4 RF from shipping emissions was calculated from Equation [4]

$$RF_{CH_4}(shipping) = RF_{CH_4}(C_{Background}) - RF_{CH_4}(C_{Background-shipping}) \quad [4]$$

A simple relationship between a change in O_3 column (Dobson Units – DU) and O_3 RF was presented by IPCC (2001). The pre-industrial global mean O_3 column was taken as 25 DU and historical O_3 forcings were also taken from IPCC (2001) to 2000, for which the RF was estimated to be 0.38 W m^{-2}. The mean forcing per DU is 0.042 W m^{-2}/DU. For future changes in column O_3 the relationship presented by IPCC (2001) between O_3 DU and NO_x, CH_4, CO and VOC emissions was used:

$$\delta(\mathrm{O}_3)_t = +5.0\delta\ln(CH_4)_{t-1} + 0.125\delta(e-NO_X)_t + 0.0011\delta(e-CO)_t + 0.0033\delta(e-VOC)_t \quad [5]$$

where $(O_3)_t$ is the tropospheric O_3 at time t (DU), CH_4 (ppbv), $(e\text{-}NO_x)_t$ are the anthropogenic NO_x emissions at time t (Tg(N)/yr); $(e\text{-}CO)_t$ are the anthropogenic CO emissions at time t (Tg/yr), and $(e\text{-}VOC)_t$ are the anthropogenic VOC emissions at time t (Tg/yr).

It was also assumed that the natural emissions of CH_4, NO_x, CO and VOC remain constant. Therefore, the emissions scenario describes all changes in emissions.

It was assumed that equation [5] predicts background tropospheric O_3 (in DU) relative to the year 2001 and the same equation was used to calculate the shipping component, using shipping emissions of NO_x, CO, CH_4 and VOCs. Therefore, the O_3 concentrations arising from shipping are assumed to be the difference between the background and shipping O_3 concentrations as in Equation [5]. The RF from the O_3 perturbation was calculated using Equation [6].

$$(RF_{\mathrm{O}_3})_t = 0.042 \times \delta(\mathrm{O}_3) + (RF_{\mathrm{O}_3})_{2000} \quad [6]$$

3 RESULTS

Two time-evolved CO_2 RF responses from shipping have been calculated from the emission datasets (i.e. EN2007, and EN2007+EY2005a) to 2000. The emissions are shown in Figure 1a and the subsequent CO_2 RF in Figure 1b. The time-evolution of emissions is evidently quite different over the period 1940 to 2000, with the estimates of EY2005a being based on interpolation of individual years (1950, 1960, 1970, 1980, 1995 and 2001), such that the reductions and subsequent increases between 1980 and 1990 as shown by EN2007 are not featured. By contrast, the emissions estimates of EN2007 between 1940 and 1975 are greater than those of EY2005a. These two features in the data have a cancelling effect in the CO_2 RF (Figure 2) by 2000 such that they reach approximately the same value of ~0.0425 W m^{-2}.

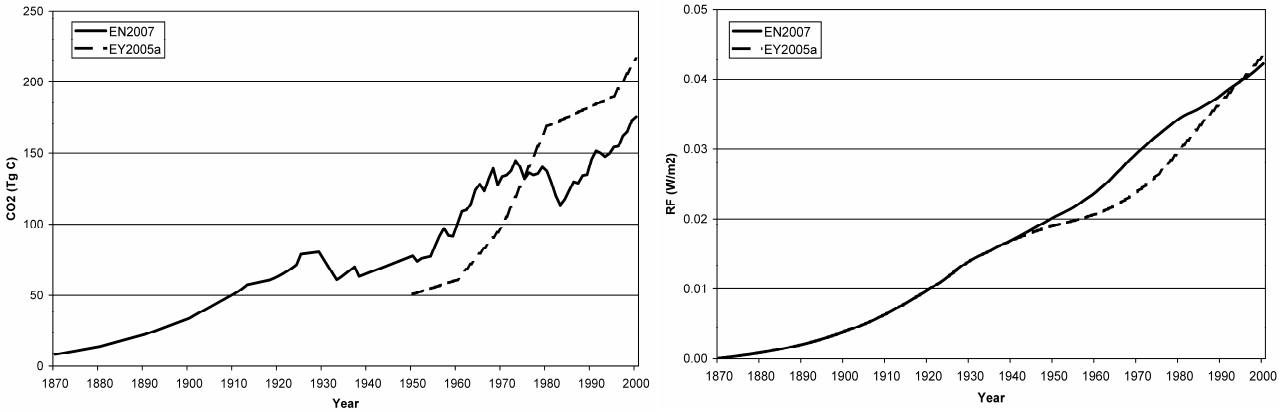

Figure 1. Panel a. Emissions of CO_2 from shipping between 1870 and 2000 according to EY2005a and EN2007, including back-extrapolation from 1925 to 1870. Panel b. Radiative forcing of CO_2 from shipping according to estimates of EY2005a and EN2007, including back-extrapolation from 1925 to 1870.

4 DISCUSSION

4.1 *An estimation of the total radiative forcing impact from shipping in 2000*

The model can be used to estimate RFs from shipping for CO_2, O_3 and CH_4, and SO_4. Currently, it does not have BC and the indirect aerosol effect implemented. If shipping RFs for 2000 calculated here are combined with independent estimates of these RFs not calculated in the model, an overall RF chart for 2000 can be given in a similar fashion (Figure 2) to those presented for aviation (IPCC, 1999; Sausen et al., 2005).

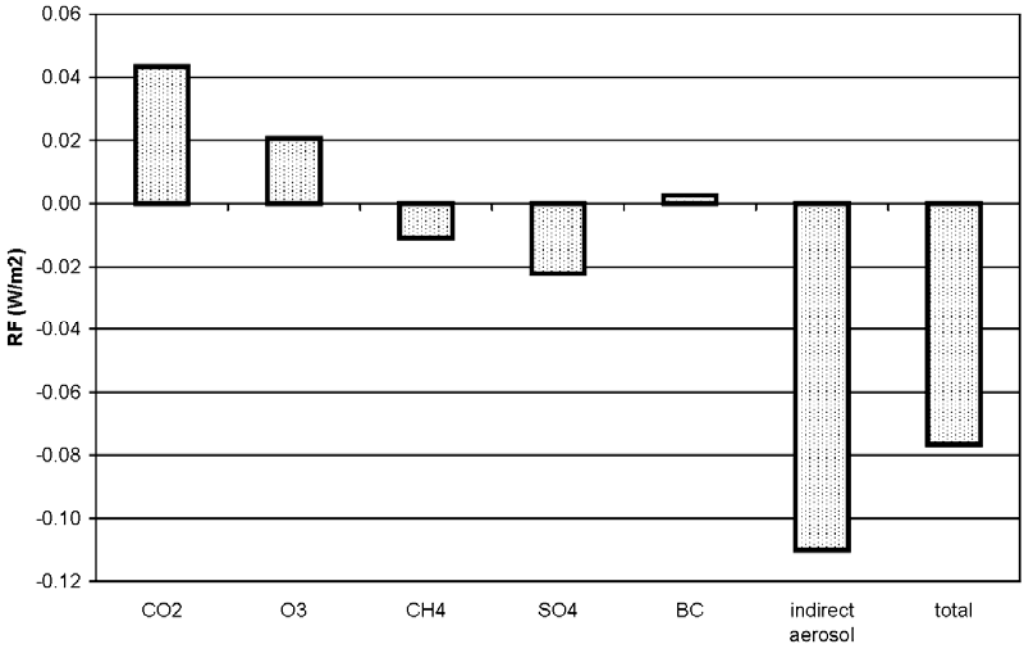

Figure 2. Radiative forcing from shipping effects in 2000: CO_2, O_3, CH_4 responses as calculated with the linear response model; BC and the indirect effect from Berntsen (2004) and Capaldo et al. (1999).

The O_3 RF was calculated to be 0.021 W m^{-2}. This is approximately twice the value of 0.0098 ± 0.002 W m^{-2} calculated by Eyring et al. (2007) using a suite of chemical transport models (CTMs). However, the emissions used by Eyring et al. (2007) were approximately one half those (in 2000) used in this study (3.10 TgN instead of 6.51 Tg N yr^{-1}), such that the response scales linearly.

Since the negative RFs from the direct effect of SO_4 and the indirect effect dominate, the total RF is negative, implying an overall cooling on a global mean basis. However, it is questionable as to whether such a global mean additivity is meaningful where strong positive and negative forcings are involved, some of which are spatially heterogeneous – this is basically a question over the usefulness of the RF metric which is a subject of debate for issues such as this. An overall negative RF from shipping that comprises both positive and negative forcings could mistakenly be interpreted as either being benign, or even *in extremis* counteracting other positive RFs. The fallacy of this interpretation is that if the sulphur in the fuel were removed, then the negative SO_4 RF would disappear in a matter of weeks, and a similar response is possible for the overall indirect aerosol effect due to shipping. In such a case where S was reduced, and the RF from this effect reduced, one would still be left with a long-term positive RF and warming from historical CO_2 emissions.

4.2 *A comparison of shipping and aviation CO_2 radiative forcing and temperature response*

It is of interest to compare aviation with shipping effects on climate since the international emissions from both of these sectors are not covered by the Kyoto Protocol because of the complication of allocating emissions. Here, only the CO_2 RF and temperature responses for shipping and aviation are compared. A more comprehensive comparison of RF effects is not yet possible because of limited emissions data availability.

In the comparison made here, the responses from the 'beginning' of shipping and aviation, i.e. 1870 and 1940 were calculated for a range of scenarios through to 2050, and thereafter to 2100 for

a single scenario. In 2000, the CO_2 RF from shipping was approximately 1.8 times that of aviation's CO_2 RF. However, the assumed growth of aviation and shipping CO_2 emissions means that the difference between the RFs diminishes and starts to converge by 2100.

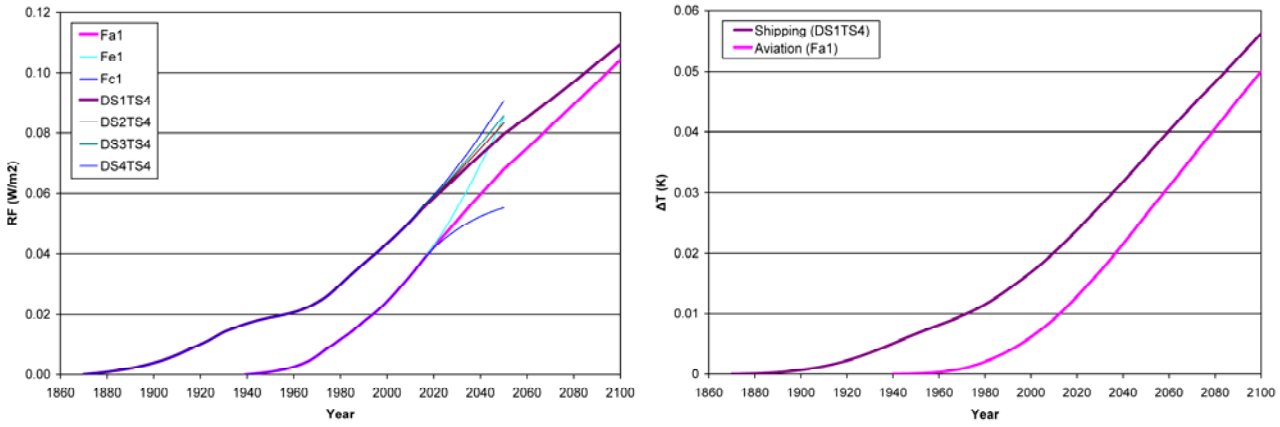

Figure 3. Panel a. Time evolution of CO_2 radiative forcing from shipping and aviation from 1870 and 1940, respectively, to 2050 under assumptions of central emission scenarios, thereafter linearly extrapolated to 2100. Panel b. Time evolution of CO_2 temperature response from shipping and aviation from 1870 and 1940, respectively, to 2050 under assumptions of central emission scenarios, thereafter linearly extrapolated to 2100.

If Figure 3b is examined for the temperature response effect on climate from these sectoral CO_2 emissions, the shipping temperature effects is a factor of ~2.7 times that of aviation in 2000 and ~1.1 times that of aviation in 2100.

4.3 *Future work and limitations of the modelling approach*

The purpose of the model is to calculate *time-evolved* RFs for the calculation of temperature response(s). For some forcing agents such as CO_2, O_3 and CH_4, the RFs can be calculated explicitly, albeit in a parameterized manner. For other agents such as the direct effect from SO_4 and BC or the indirect aerosol effect, individual yearly values may be used with some parameter (such as fuel) to scale these RFs over time in order to calculate temperature responses. As independent estimates of some of these forcing effects become available, they will be implemented in the model. Whilst the RF response to shorter-lived climate forcing agents such as O_3, SO_4 etc. is relatively fast, it should be remembered that the *temperature* response to these forcings is longer because of the thermal inertia of the climate system arising from the slow exchange times of heat between the ocean and the atmosphere. In the future, a complete history of emissions of NO_x, CO, VOCs and CH_4 are needed to calculate the temperature response from shipping-induced changes in O_3 and CH_4 RFs.

The nature of the model has limitations that should be born in mind when interpreting the output: it is a *global mean* model, such that it is a robust method to calculate temperature response for homogeneous forcings (assuming that it is appropriately tuned to some GCM). For other forcings such as O_3, BC, SO_4 or the indirect aerosol effect, the spatial forcing is highly heterogeneous and it is not necessarily the case that a global mean response is entirely appropriate for interpreting the overall temperature response to, e.g., shipping emissions in an additive manner. However, to a first order, such global mean models can produce useful initial data for a first-order interpretation of the impacts of a transport sector such as shipping.

5 CONCLUSIONS

- This study addresses time-evolved RFs and temperature responses from some of the effects of shipping, particularly CO_2, O_3 and CH_4.
- A robust estimate of shipping CO_2 RF has been made for 2000 with the usage of a full history of shipping's emissions of 0.043 W m^{-2}. A shipping O_3 RF of 0.021 W m^{-2} in 2000 has been calculated using a simple method, which is in agreement with independent calculations using complex

3D chemical transport models, allowing for a linear scaling of emissions. Shipping NO_x emissions result in a negative CH_4 RF of -0.01 W m^{-2} in 2000, as calculated with a simplified methodology.
- Combining these RFs with others not calculated with the model result in an overall global mean RF due to shipping in 2000 of approximately -0.08 W m^{-2}.
- Shipping CO_2 RF was approximately 1.8 times that of aviation in 2000 and the resultant temperature response of (CO_2 only) for shipping was found to be 2.7 times that of aviation in 2000.

6 ACKNOWLEDGEMENTS

This work is a contribution to the EU Sixth Framework Project 'Quantify', contract no.003893 (GOCE). DSL and LL (MMU) were additionally funded by UK Dft & DTi; RS and VE (DLR) were funded by the Quantify project and the Helmholtz-University Young Investigators Group SeaKLIM. ØE and HLB (DNV) were funded by the Quantify project.

7 REFERENCES

Berntsen T. 2004: impacts of aviation and other transport modes on the atmosphere: a European perspective. Presentation at NERC Town Meeting, 'Aviation Impacts on the Atmosphere', 11-12th November, Birkbeck College, NCAS workshop, UK.

Capaldo K., Corbett J. J., Kasibhatla P., Fischbeck P and Pandis S. N. 1999: Effects of ship emissions on sulphur cycling and radiative climate forcing over the ocean. *Nature* 400, 743 – 746.

Endresen, Ø., E. Sørgård , J. K. Sundet, S. B. Dalsøren, I. S. A. Isaksen, T. F. Berglen, and G. Gravir,. 2003: Emission from international sea transportation and environmental impact. *J. Geophys. Res.* 108, 4560, doi:10.1029/2002JD002898.

Endresen Ø., P. O. Brett, H. L. Behrens, E. Sogård and I. S. A. Isaksen, 2006: A historical reconstruction of ships energy consumption and emissions. *J. Geophys. Res.* (submitted).

Eyring, V., H.W. Köhler, J. van Aardenne, and A. Lauer 2005a: Emissions from international shipping: 1. The last 50 years. *J. Geophys. Res.* 110, D17305, doi:10.1029/2004JD005619.

Eyring, V., H. W. Köhler, A. Lauer, and B. Lemper 2005b: Emissions from international shipping: 2. Impact of future technologies on scenarios until 2050. *J. Geophys. Res*., 110, D17306, doi:10.1029/2004JD005620.

Eyring, V., D. S. Stevenson, A. Lauer, F. J. Dentener, T. Butler, W. J. Collins, K. Ellingsen, M. Gauss, D. A. Hauglustaine, I. S. A. Isaksen, M. G. Lawrence, A. Richter, J. M. Rodriguez, M. Sanderson, S. E. Strahan, K. Sudo, S. Szopa, T. P. C. van Noje and O. Wild 2007: Multi-model simulations of the impact of international shipping on atmospheric chemistry and climate in 2000 and 2030. *Atmos. Chem. Phys., accepted.*

Hasselmann K., R. Sausen, E. Maier-Reimer, and R. Voss, 1993: On the cold start problem in transient simulations with coupled atmosphere-ocean models. *Clim. Dynamics* 9, 53–61.

IPCC 1999: Aviation and the global atmosphere, J.E. Penner, D.H. Lister, D.J. Griggs, D.J. Dokken, M. McFarland (Eds), Cambridge University Press, Cambridge, UK.

IPCC 2001: Climate change 2001: The Scientific Basis. Contribution of Working Group 1 to the Third Assessment Report, J.T. Houghton (Eds), Cambridge University Press, Cambridge, UK.

Lim L. L., D. S. Lee, R. Sausen, and M. Ponater 2007: Quantifying the effects of aviation on radiative forcing and temperature with a climate response model. *Clim. Change* (submitted).

Sausen R. and U. Schumann, 2000: Estimates of the climate response to aircraft CO_2 and NO_x emissions scenarios. *Clim. Change* 44, 27-58.

Sausen R., I. Isaksen, V. Grewe, D. Hauglustaine, D. S. Lee, G. Myhre, M. O. Köhler, G. Pitari, U. Schumann, F. Stordal, and C. Zerefos, 2005: Aviation radiative forcing in 2000: and update on IPCC (1999). *Met. Zeitschrift* 114, 555–561.

Schreier, M., A. A. Kokhanovsky, V. Eyring, L. Bugliaro, H. Mannstein, B. Mayer, H. Bovensmann, and J. P. Burrows, 2006: Impact of ship emissions on the microphysical, optical and radiative properties of marine stratus: a case study. *Atmos. Chem. Phys.*6, 4925–4942.

Contrails, contrail cirrus, and ship tracks

K. Gierens*
DLR-Institut für Physik der Atmosphäre Oberpfaffenhofen, Germany

Keywords: Aerosol effects on clouds and climate

ABSTRACT: The following text is an enlarged version of the conference tutorial lecture on contrails, contrail cirrus, and ship tracks. I start with a general introduction into aerosol effects on clouds. Contrail formation and persistence, aviation's share to cirrus trends and ship tracks are treated then.

1 INTRODUCTION

The overarching theme above the notions "contrails", "contrail cirrus", and "ship tracks" is the effects of anthropogenic aerosol on clouds and on climate via the cloud's influence on the flow of radiation energy in the atmosphere. Aerosol effects are categorised in the following way:

- Direct effect: Aerosol particles scatter and absorb solar and terrestrial radiation, that is, they interfere directly with the radiative energy flow through the atmosphere (e.g. Haywood and Boucher, 2000).
- Semidirect effect: Soot particles are very effective absorbers of radiation. When they absorb radiation the ambient air is locally heated. When this happens close to or within clouds, the local heating leads to buoyancy forces, hence overturning motions are induced, altering cloud evolution and potentially lifetimes (e.g. Hansen et al., 1997; Ackerman et al., 2000).
- Indirect effects: The most important role of aerosol particles in the atmosphere is their role as condensation and ice nuclei, that is, their role in cloud formation. The addition of aerosol particles to the natural aerosol background changes the formation conditions of clouds, which leads to changes in cloud occurrence frequencies, cloud properties (microphysical, structural, and optical), and cloud lifetimes (e.g. Lohmann and Feichter, 2005).

Water clouds always form right at water saturation because there are always enough aerosol particles present, so that the vapour can immediately condense and form droplets. The addition of anthropogenic aerosol, for water clouds therefore leads to more numerous but smaller droplets (Twomey effect, Twomey, 1974, 1977). Since radiation scattering gets stronger with decreasing droplet size (when the water mass stays constant) the Twomey effect makes clouds more reflective of solar radiation. Ship tracks are a good example of this effect. Since the droplets get smaller when additional aerosol is present, their tendency to fall relative to the air will be reduced. This weakens the cloud's tendency to form drizzle.

Ice clouds are more complicated than water clouds, because they do not form right at ice saturation. Instead, the natural way of cirrus formation is freezing of supercooled aqueous solution droplets, which needs supersaturations of 45% and more, depending on temperature. Ice nuclei (from anthropogenic sources) that commence to form ice at lower supersaturations may inhibit the build-up of the large supersaturations necessary for freezing of the solution droplets. This generally leads to less and larger ice crystals with a corresponding higher tendency to precipitate. Aerosol particles from aviation could act in this way, but this is yet a hypothesis.

Contrails can form in the blue sky when the ambient air is not supersaturated enough to allow natural formation of cirrus. In the wake of an aircraft, the humidity can reach transiently very high supersaturation, sufficient to let the exhaust particles act as condensation nuclei. Once formed, the contrail ice crystals (at least a fraction of them) can survive as soon as the ambient air is supersaturated. In such a case the contrail can grow laterally into a so-called contrail cirrus, i.e. a naturally

* *Corresponding author:* Klaus Gierens, DLR-Institut für Physik der Atmosphäre, Oberpfaffenhofen, D-82205 Wessling, Germany. Email: Klaus.Gierens@dlr.de

looking cirrus cloud that would not exist without the prior formation of a contrail. This kind of cirrus formation occurs quite frequently.

2 CONTRAILS AND CONTRAIL CIRRUS

2.1 *Contrail formation*

Contrail formation is like breathing in cold air: Mixing of hot and moist exhaust gases with sufficiently cold ambient air can lead to transient water supersaturation. Exhaust particles and ambient aerosol particles entrained by the vigorous swirling vortex act as condensation nuclei, the supersaturated vapour condenses and quickly freezes in the cooling mixture. Contrail formation takes about 1/3 s.

Whether or not a contrail forms can be decided by the Schmidt-Appleman criterion (Schumann, 1996), a thermodynamic criterion that says that the mixture of the exhaust gases with ambient air must achieve supersaturation with respect to water. In-flight tests of the Schmidt-Appleman criterion have shown its validity (Busen and Schumann, 1995; Jensen et al., 1998; Kärcher et al., 1998). The fact that water saturation must be reached and that ice saturation is not sufficient for contrail formation is due to the poor ice nucleating efficiency of the exhaust particles.

An interesting consequence of the Schmidt-Appleman theory is that modern aircraft can produce contrails in warmer air than old aircraft, that is at lower altitudes (Schumann, 2000; Schumann et al. 2000). The reason behind that is that the exhaust gases of modern, more efficient, engines are cooler than those of old engines (a larger fraction of the fuel energy is used for propulsion), so that water saturation can be achieved in warmer ambient conditions.

Another way of contrail formation is by the aerodynamic cooling of the air flowing over the wing (see Gierens et al., this volume). This process is independent of the Schmidt-Appleman criterion.

2.2 *Contrail-to-Cirrus transition*

The Schmidt-Appleman criterion says only whether or not a contrail can form. It says nothing about the persistence of a contrail. Whether a contrail is persistent or not depends on the ambient relative humidity with respect to ice. One should note that water supersaturation is required only for a fraction of a second during the mixing process to trigger droplet condensation; in principle, a contrail can be formed even in totally dry air, yet a very short one. A contrail can survive until the wake vortices burst (after about 2 min) when the humidity is closer to but below ice saturation. Such a condition can easily be recognized by a ground observer by watching how the contrail evolves into closed rings that quickly vanish. An example is given in Figure 1.

Figure 1. Short non-persistent contrail that forms vortex rings and evaporates then (source: DLR).

Contrail persistence beyond the lifetime of the vortices requires ice supersaturation. Ice supersaturation is a relatively frequent phenomenon in the upper troposphere; it even occurs sometimes in the stratosphere, just above the tropopause. From MOZAIC data we can derive that commercial air traffic routes are about 15% of their way in ice supersaturated air masses (Gierens et al., 1999). Ice supersaturated regions have a mean horizontal extension of 150 km, but specimen with extensions of several thousand kilometres have been found (Gierens and Spichtinger, 2000). Their mean vertical extension is about half a kilometre, at least over Lindenberg in eastern Germany where the measurements took place (Spichtinger et al., 2003). Lifetimes exceeding a day have been found in case studies (Spichtinger et al., 2005), and a few days lifetime of contrail clusters have been found in satellite imagery as well (Bakan et al., 1994).

Contrail-to-cirrus transition starts with the break-up of the vortices. The number of ice crystals that survive the vortex phase is an important initial condition for contrail-to-cirrus transition, as well as the vertical extent and distribution of the ice in the contrail. Both depend strongly on aircraft parameters and ambient conditions, in particular, the degree of supersaturation and temperature. For instance, the fraction of ice crystals surviving the vortex phase is nearly zero just at saturation, and increases to nearly all at about 10-20% supersaturation. Unterstrasser et al. (this volume) give more details on this. The large variability of initial conditions for contrail-to-cirrus transition probably implies a large variation in the properties of the resulting contrail cirrus. The prime mechanism of the transition is spreading of the contrail due to vertical variation of horizontal wind speed, the wind shear. Spreading rates increase with increasing wind shear and with increasing initial vertical extension of the contrail (Dürbeck and Gerz, 1996; Gerz et al., 1998). Horizontal spreading rates ranging from 18 to 140 m/min have been measured with a scanning lidar (Freudenthaler et al., 1995; Freudenthaler, 2000). In a case study, Duda et al. (2004) estimated contrail spreading rates of 2.7 km/h from satellite imagery and weather forecast wind fields.

The later evolution of contrail cirrus depends on the spreading rates and the ambient humidity field. Spreading alone implies dispersion of the ice crystals over a large area, decreasing the optical thickness of the contrail. However, the crystals grow in the supersaturated air, and fresh moisture is mixed into the contrail during the spreading process. The ice mass per crystal increases, and so does the optical thickness. At the same time, the growing crystals may grow enough to eventually fall out of the ice supersaturated region and to evaporate, again decreasing the optical thickness of the contrail cirrus. Usually, persistent contrails don't appear as single objects, and the spreading of several contrails finally leads to a contrail deck (Gierens, 1998) in which the evolution of one contrail cannot be considered separately from the others. Contrail decks also often evolve close to natural cirrus clouds. There is not much known about the evolution of contrail decks nor about the evolution of contrails close to or within cirrus clouds.

2.3 *Aviation's share of cirrus trends*

A long-standing question in relation to air traffic has been whether aviation increases the average cloudiness and whether it affects other weather parameters like daily sunshine duration and temperature range. Here I concentrate on studies that relate aviation with trends of cirrus cloudiness.

Boucher (1999) took ground and ship based cloud observations of the period 1982-1991, grouped into early (1982-1986) and late (1987-1991). He then correlated the late minus early differences of cirrus frequency of occurrence, ΔC, in $3° \times 3°$ grid boxes with the aviation fuel consumption, F, in the same area. He found that essentially ΔC increases with F. Highest ΔC occurred in main air flight corridors, NE USA (+13.3%/decade), and North Atlantic Flight Corridor (+7.1%/decade). Boucher stated that effects of volcanoes, long term changes in relative humidity, or climate variations related to the North Atlantic Oscillation (NAO) could not solely explain the trend in C, nor its regional distribution.

Minnis et al. (2001) performed a similar study, adding satellite data. They found consistency in trends of cirrus and contrails over USA, but not so over Europe, which could point to other important influences on cloudiness, that are stronger in Europe than in USA.

Zerefos et al. (2003) took other potential influence factors into account in their study, namely El Niño Southern Oscillation (ENSO), NAO, and the Quasi Biennial Oscillation (QBO). They deseasonalised the cirrus time series and removed the ENSO, NAO, and QBO signals. Possible effects of changing tropopause temperatures and convective activity were removed by linear regression. Only the residuals were correlated with air traffic. These were found to increase, sometimes statistically

significantly, in regions with heavy air traffic, although an overall decrease of cirrus frequency was found. Consistent with Minnis et al., the most significant correlations were found over North America (winter season) and over the NAFC (summer season), while the correlations over Europe were insignificant (at a 95% level).

Stubenrauch and Schumann (2005) studied satellite data (1987-1995) for trends of effective high cloud amount. They introduced a new element in these studies by grouping their data into three classes, according to the retrieved upper tropospheric humidity over ice, UTHi (an average of relative humidity over a thick layer in the upper troposphere, say from 200 to 500 hPa): (1) UTHi high enough for cirrus formation; (2) UTHi not sufficient for cirrus formation, but sufficient for contrail formation; (3) clear sky. It turned out that this additional classification of the data led to a very clear positive trend (+3.7%/decade over Europe, +5.5% over NAFC) in effective high cloud amount, while the overall trend (all classes) was weak.

Stordal et al. (2005) found from an analysis of satellite data (1984-2000) that the time series of cirrus coverage C(t) and air traffic density D(t) (flown distance per km^2 and hour) are generally positively correlated. The correlation is inferred from a linear ansatz: $dC/dt = b\, dD/dt$. Estimated correlations are not strong (partly because other influences have been left in the C(t) time series). They conclude that over Europe aviation produces an extra cirrus coverage of 3 to 5%.

Mannstein and Schumann (2005) also correlated C(t) with D(t), however for 2 months of cirrus data from METEOSAT and actual air traffic data from EUROCONTROL. For relating cirrus cover and traffic density they used an ansatz that takes overlapping of contrails and saturation effects (e.g. finite size of ice-supersaturated regions) into account: $C(t) = Ci(t) + C_{pot}[1-\exp(-D/D^*)]$, where Ci(t) is cover of natural cirrus, C_{pot} is the potential coverage of persistent contrails (Sausen et al., 1998), and the term in square brackets is the fraction of C_{pot} that is actually covered by contrails. It was shown that the relation between additional cirrus coverage and air traffic density indeed followed roughly the exponential model. The main result of this study was that over Europe aviation is responsible for an additional cirrus coverage of 3% (consistent with the result of Stordal et al.). This implies that the mean coverage of contrail cirrus over Europe exceeds the corresponding mean coverage of linear contrails by almost one order of magnitude.

Krebs (2006) extended the study of Mannstein and Schumann, by analysing cirrus coverage and air traffic of 11 months in 2004, for Europe, North Africa, and the North Atlantic. Over this extended region he still found a significant correlation between cirrus coverage and air traffic density. But the air traffic induced cirrus cover was smaller than in the Mannstein and Schumann study, namely 0.6±0.2%. The inclusion of regions with essentially no air traffic of course leads to smaller mean additional cirrus coverage. Krebs also investigated the effect of the additional cirrus on the radiation budget of the earth. He found a warming of 1.1 W/m^2 for the region of interest, a value that is more than eight times larger than the value estimated by Boucher (1999). It is currently not clear how much of the correlation in this work between air traffic and cirrus cloudiness is actually due to a causal relationship. Hence the determination of the radiative forcing of contrail cirrus is fraught with very large uncertainties; studies to resolve the differences and to constrain the error margins are certainly needed.

All these studies suggest that air traffic actually induces additional cirrus clouds which seems plausible. However it is extremely difficult to demonstrate and prove such a correlation because the variation of cirrus cloudiness due to natural influences is much larger than the possible aviation effect. Hence, to look for the latter is like looking for a signal hidden in strong noise.

3 SHIP TRACKS

Ship tracks are a good example of the Twomey effect. The clean marine boundary layer (MBL) contains mainly sea salt and sulphate aerosol with a number density of about 500 cm^{-3}. When these act as condensation nuclei, a water cloud forms with a low number density of relatively large droplets. Ship stacks release a lot of soot (and other) particles into the MBL. A part of them also act as cloud condensation nuclei: more but smaller droplets form. The water content of the clouds is hardly affected. Now, the same water amount has a larger optical effect when it is distributed into more but smaller droplets (like a big block of ice can be translucent while crushed ice is opaque).

Thus, the cloud areas that are contaminated by ship emissions have a signature of higher reflectivity than their surroundings on satellite images, which is used to detect them.

The largest measurement campaign to date devoted to the study of ship tracks was conducted in June 1994 off the coast of California, the so-called Monterey Area Ship Track (MAST) Experiment (Durkee et al., 2000a). It produced the largest dataset so far of direct measurements of the effects of ship emissions on the microphysical and radiative properties of marine stratocumulus clouds as an analogue for the indirect effects of anthropogenic pollution on cloud albedo. An analysis of 131 ship-ship track correlation pairs by Durkee et al. (2000b) gave the following ship track characteristics (mean values ± standard deviation): length 296 ± 233 km, width 9 ± 5 km, age 7.3 ± 6 h (but many tracks get older than 12 h), the head of the ship track is 16 ± 8 km behind or 25 ± 15 min. after the ship. Significant variability of the values around their respective averages may be noted. Ship tracks form in a MBL that is between 300 and 750 m deep, and never deeper than 800 m during MAST. Low level clouds must be close to the surface (less than one km), otherwise ship tracks do not form (Coakley et al., 2000). The relative humidity is usually high, temperature differences between air and see are low, and winds are moderate with wind speeds of 7.7 ± 3.1 m/s. However, statistical distributions of MBL and cloud properties overlap a lot for ship track and non-ship track regions. The statistical significance of the differences in the mean have not been given for the MAST experiment.

Not all ships produce tracks. Ships powered by Diesel units that emit high concentrations of accumulation mode aerosol can produce ship tracks. Ships that produce few particles (e.g. nuclear ships) or particles too small for activation as cloud drops (even if in high concentration) do not produce ship tracks. The most likely, if not the only, cause of the formation of ship tracks is the direct emission of cloud condensation nuclei from the stack of a Diesel powered ship. Still then it needs a cloud layer susceptible to aerosol perturbation, and the atmospheric stability must be such to enable aerosol to be mixed throughout the MBL. Furthermore, not all exhausted particles are active as additional cloud condensation nuclei. The type of fuel burned seems to be more important than the type of ship engine in determining whether a ship will produce a track or not. Ships, burning Marine Fuel Oil (a low-grade oil) or navy distillate fuel (high-grade) produce between 4×10^{15} to 2×10^{16} particles per kg fuel burned. About 12% of the particles from Marine Fuel Oil burning serve as cloud condensation nuclei, whereas burning of higher-grade fuels produces particles that are less efficient as cloud condensation nuclei. Ship exhaust particles are composed primarily from organics, possibly combined with H_2SO_4 generated by gas-to-particle conversion from SO_2. 10% (by mass) are water soluble materials. There is no evidence that salt particles from ship wakes cause ship tracks. Water and heat fluxes do not produce detectable perturbations that have an effect on MBL clouds (Hobbs et al., 2000).

As the droplets in a ship track are smaller than usual in a MBL cloud, their coagulation rate to form larger droplets that eventually precipitate in the form of drizzle is diminished. In other words, ship tracks suppress drizzle formation which affects cloud life time and the budget of latent heat. As drizzle formation causes the transition from closed to open cellular convection (Rosenfeld et al., 2006), this transition does not occur in ship tracks. Analysis of satellite data (Schreier et al., 2006) with comparison between non-ship-track pixels and ship-track pixels shows a large increase in the droplet number concentration from 100 cm^{-3} to 800 cm^{-3}. Since the condensed water mass is probably unaffected by the ship track (the satellite data shows that the liquid water path is hardly affected), the droplet's effective radius experiences a significant decrease of from 12 to 6 μm, a clear indication of the Twomey effect. Accordingly, the optical thickness of unpolluted clouds is 20-30, whereas in the ship track it increases up to 45.

Comparing the ocean regions where ship tracks occur with the regions where ship traffic occurs shows that ship tracks is a very selective phenomenon. The special combination of meteorological conditions necessary for formation of ship tracks is rarely given. Thus the direct radiative impact of ship tracks on the Earth's energy budget is probably small. However, ship emissions can have more diffuse effects on low-level clouds that might be of higher climatic relevance, although much harder to detect. Devasthale et al. (2006) analysed time series of satellite data of the region around the English Channel (an ocean strait with very heavy ship traffic) and detected trends of cloud albedo and top temperature, that were ascribed to increasing ship emissions.

4 CONCLUSIONS

Clouds are of utmost importance in the climate system because of their interaction with the hydrological cycle and the radiant energy flow. The transportation sector may cause changes in cloud coverage and frequency and changes in cloud properties. These influences are exerted via semi-direct and indirect aerosol effects. Research currently is focused on ship and aviation emissions and does not include the impact of road traffic emissions on clouds. This is because of the following two reasons: (1) There are evident cloud effects from both shipping (ship tracks) and aviation (contrails) whereas there are no evident cloud effects from road traffic. (2) The road traffic source is rather diffuse (many cars almost everywhere in Europe) whereas aviation is more regulated and shipping by large vessels is more confined to distinct routes. Their movements are recorded which makes source attribution better identified than it would be the case for road traffic. Nevertheless, future research must take the cloud effects of surface transport and of industrial emissions into account, in order to enable fair comparisons of the effects. The knowledge gained from current research on contrails, contrail cirrus, and ship tracks will certainly help for the future topics.

REFERENCES

Ackerman, A. S., O. B. Toon, D. E. Stevens, A. J. Heymsfield, V. Ramanathan, and E. J. Welton, 2000: Reduction of tropical cloudiness by soot. *Science, 288,* 1042–1047.

Bakan, S., M. Betancor, V. Gayler, and H. Graßl, 1994: Contrail frequency over Europe from NOAA-satellite images. *Ann. Geophys., 12,* 962–968.

Boucher, O., 1999: Air traffic may increase cirrus cloudiness. *Nature, 397,* 30–31.

Busen, R., and U. Schumann, 1995: Visible contrail formation from fuels with different sulfur contents. *Geophys. Res. Lett., 22,* 1357–1360.

Coakley Jr., J.A., and 10 co-authors, 2000: The appearance and disappearance of ship tracks on large spatial scales. *J. Atmos. Sci., 57,* 2765–2778.

Devasthale, A., O. Krüger, and H. Graßl, 2006: Impact of ship emissions on cloud properties over coastal areas. *Geophys. Res. Lett., 33,*L02811, doi:10.1029/2005GL024470.

Duda, D.P., P. Minnis, L. Nguyen, and R. Palikondra, 2004: A case study of the development of contrail clusters over the Great Lakes. *J. Atmos. Sci., 61,* 1132–1146.

Dürbeck, T., and T. Gerz, 1996: Dispersion of aircraft exhausts in the free troposphere. *J. Geophys. Res., 101,* 26007–26015.

Durkee, P.A., K.J. Noone, and R.T. Bluth, 2000a: The Monterey Area Ship Track experiment. *J. Atmos. Sci., 57,* 2523–2541.

Durkee, P., A., R.E. Chartier, A. Brown, E.J. Trehubenko, S.D. Rogerson, C. Skupniewicz, K.E. Nielsen, S. Platnick, and M.D. King, 2000b: Composite ship track characteristics. *J. Atmos. Sci., 57,* 2542–2553.

Freudenthaler, V., F. Homburg, and H. Jäger, 1995: Contrail observations by ground-based scanning lidar: Cross-sectional growth. *Geophys. Res. Lett., 22,* 3501–3504.

Freudenthaler, V., 2000: Lidarmessungen der räumlichen Ausbreitung sowie mikrophysikalischer und optischer Parameter von Flugzeugkondensstreifen. Dissertation, Schriftenreihe des Fraunhofer Instituts Atmosphärische Umweltforschung, Garmisch-Partenkirchen, Band 63-2000, 135 pp. (in German).

Gerz, T., T. Dürbeck, and P. Konopka, 1998: Transport and effective diffusion of aircraft emissions. *J. Geophys. Res., 103,* 25905–25913.

Gierens, K.M., 1998: How the sky gets covered with contrails. *Meteorol. Z., N.F. 7,* 181–187.

Gierens, K., U. Schumann, M. Helten, H.G.J. Smit, and A. Marenco, 1999: A distribution law for relative humidity in the upper troposphere and lower stratosphere derived from three years of MOZAIC measurements. *Ann. Geophys., 17,* 1218–1226.

Gierens, K., and P. Spichtinger, 2000: On the size distribution of ice-supersaturated regions in the upper troposphere and lowermost stratosphere. *Ann. Geophys., 18,* 499–504.

Gierens, K., B. Kärcher, H. Mannstein, and B. Mayer, 2006: Aerodynamically induced contrail formation, this volume.

Hansen, J., M. Sato, and R. Ruedy, 1997: Radiative forcing and climate response. *J. Geophys. Res., 102,* 6831–6864.

Haywood, J. M., and O. Boucher, 2000: Estimates of the direct and indirect radiative forcing due to tropospheric aerosols: A review. *Rev. Geophys., 38,* 513–543.

Hobbs, P.V., and 13 co-authors, Emissions from ships with respect to their effects on clouds. *J. Atmos. Sci., 57,* 2570–2590.

Jensen, E.J., O.B. Toon, S. Kinne, G.W. Sachse, B.E. Anderson, K.R. Chan, C. Twohy, B. Gandrud, A. Heymsfield, and R.C. Miake-Lye, 1998: Environmental conditions required for contrail formation and persistence. *J. Geophys. Res., 103,* 3929–3936.

Kärcher, B., R. Busen, A. Petzold, F.P. Schröder, U. Schumann, and E.J. Jensen, 1998: Physicochemistry of aircraft-generated liquid aerosols, soot, and ice particles. 2. Comparison with observations and sensitivity studies. *J. Geophys. Res., 103,* 17129–17148.

Krebs, W., 2006: Analyse des Einflusses des Flugverkehrs auf die natürliche Zirrusbewölkung über Europa, Nordafrika und dem Nordatlantik. Dissertation, Ludwig–Maximilians Universität München, 211 pp. (in German).

Lohmann, U., and J. Feichter, 2005: Global indirect aerosol effects: a review. *Atmos. Chem. Phys., 5,* 715–737.

Mannstein, H., and U. Schumann, 2005: Aircraft induced contrail cirrus over Europe. *Meteorol. Z., 14,* 549–554.

Minnis, P., J.K. Ayers, R. Palikondra, D.R. Doelling, U. Schumann, and K. Gierens, 2001: Changes in cirrus cloudiness and their relationship to contrails. Proceedings American Meteorological Society, Boston, USA, No. 11.9, 239–242.

Rosenfeld, D., Y.J. Kaufman, and I. Koren , 2006: Switching cloud cover and dynamical regimes from open to closed Benard cells in response to the suppression of precipitation by aerosols. *Atmos. Chem. Phys., 6,* 2503–2511.

Sausen, R., K. Gierens, M. Ponater, and U. Schumann, 1998: A diagnostic study of the global distribution of contrails, Part I. Present day climate. *Theor. Appl. Climatol., 61,* 127–141.

Schreier, M., A.A. Kokhanovsky, V. Eyring, L. Bugliaro, H. Mannstein, B. Mayer, H. Bovensmann, and J.P. Burrows, 2006: Impact of ship emissions on the microphysical, optical and radiative properties of marine stratus: a case study. *Atmos. Chem. Phys., 6,* 4925–4942.

Schumann, U., 1996: On conditions for contrail formation from aircraft exhausts. *Meteorol. Z., N.F. 5,* 4–23.

Schumann, U., 2000: Influence of propulsion efficiency on contrail formation. *Aerospace Sci. Technol., 4,* 391–401.

Schumann, U., R. Busen, and M. Plohr, 2000: Experimental test of the influence of propulsion efficiency on contrail formation. *J. Aircraft, 37,* 1083–1087.

Spichtinger, P., K. Gierens, U. Leiterer, and H. Dier, 2003: Ice supersaturated regions over Lindenberg, Germany. *Meteorol. Z., 12,* 143–156.

Spichtinger, P., K. Gierens, H. Wernli, 2005: A case study on the formation and evolution of ice supersaturation in the vicinity of a warm conveyor belt's outflow region. *Atmos. Chem. Phys., 5,* 973–987.

Stordal, F., G. Myhre, E.J.G. Stordal, W.B. Rossow, D.S. Lee, D.W. Arlander, and T. Svendby, 2005: Is there a trend in cirrus cloud cover due to aircraft traffic? *Atmos. Chem. Phys., 5,* 2155–2162.

Stubenrauch, C.J., and U. Schumann, 2005: Impact of air traffic on cirrus coverage. *Geophys. Res. Lett., 32,* L14813, doi:10.1029/2005GL022707.

Twomey, S., 1974: Pollution and the planetary albedo. *Atmos. Environ., 8,* 1251–1256.

Twomey, S., 1977: The influence of pollution on the shortwave albedo of clouds. *J. Atmos. Sci., 34,* 1149–1152.

Unterstrasser, S., K. Gierens, and P. Spichtinger, 2006: Initial conditions for contrail-to-cirrus transition. This volume.

Zerefos, C.S., K. Eleftheratos, D.S. Balis, P. Zanis, G. Tselioudis, and C. Meleti, 2003: Evidence of impact of aviation on cirrus cloud formation. *Atmos. Chem. Phys., 3,*1633–1644.